VAL genes regulate vegetative phase change via miR156-dependent and independent mechanisms

Jim P. Fouracre[1], Jia He[1,3], Victoria J. Chen[1], Simone Sidoli[2] and R. Scott Poethig[1]*

[1] Biology Department, University of Pennsylvania, Philadelphia, Pennsylvania, 19104, USA

[2] Department of Biochemistry, Albert Einstein College of Medicine, Bronx, New York 10461, USA

[3] Current address: Cold Spring Harbor Laboratory, Cold Spring Harbor, New York 11724, USA

* Corresponding author: Poethig, R. S. (spoethig@sas.upenn.edu)

Abstract

How organisms control when to transition between different stages of development is a key question in biology. In plants, epigenetic silencing by Polycomb repressive complex 1 (PRC1) and PRC2 plays a crucial role in promoting developmental transitions, including from juvenile-to-adult phases of vegetative growth. PRC1/2 are known to repress the master regulator of vegetative phase change, miR156, leading to the transition to adult growth, but how this process is regulated temporally is unknown. Here we investigate whether transcription factors in the *VIVIPAROUS/ABI3-LIKE* (*VAL*) gene family provide the temporal signal for the epigenetic repression of miR156. Exploiting a novel *val1* allele, we found that *VAL1* and *VAL2* redundantly regulate vegetative phase change by controlling the overall level, rather than temporal dynamics, of miR156 expression. Furthermore, we discovered that *VAL1* and *VAL2* also act independently of miR156 to control this important developmental transition.

Introduction

Flowering plant development is underpinned by transitions between stereotypical stages of growth: embryogenesis, seed maturation, juvenile and adult phases of vegetative development and flowering (Huijser and Schmid, 2011). The correct timing of these transitions is critical to plant survival and, ultimately, reproductive success. Vegetative phase change describes the transition from juvenile-to-adult vegetative growth and is associated with changes to multiple traits, including leaf morphology, light-use efficiency, herbivore resistance and shoot physiology (Gou et al., 2011; Lawrence et al., 2020; Leichty and Poethig, 2019; Mao et al., 2017). In *Arabidopsis thaliana*, the juvenile phase is characterized by small round leaves that lack both trichomes on the abaxial surface and serrations. Adult leaves, on the other hand, are larger, more elongated, serrated and produce abaxial trichomes (Telfer et al., 1997).

Vegetative phase change is triggered by activity of members of the *SQUAMOSA PROMOTER BINDING PROTEIN-LIKE* (*SPL*) family of transcription factors, which are post-transcriptionally repressed during juvenile development by the microRNAs miR156/miR157 (Fouracre and Poethig, 2019; Wu and Poethig, 2006; Wu et al., 2009; Xu et al., 2016a). miR156/miR157 are encoded by multiple genes of which *MIR156A* and *MIR156C* are the most functionally significant (He et al., 2018). The expression of *MIR156A* and *MIR156C* declines during juvenile growth (Yang et al., 2013b; Yu et al., 2013), leading to the de-repression of their *SPL* targets and the transition to adult growth. Elucidating what controls the decline in *MIR156A*/*C* expression is therefore critical to understanding how the juvenile-to-adult transition is regulated in plants.

The molecular mechanisms that lead to the temporal repression of *MIR156A/C* are only beginning to be understood. The activity of Polycomb Group (PcG) transcriptional repressors appears critical. There are two functional complexes of PcG proteins in plants, both of which repress gene expression through covalent histone modifications. PcG repressive complex 1 (PRC1) consists of a H2A E3 ubiquitin ligase module containing one AtBMI1 protein (AtBMI1A/B/C) and one AtRING1 protein (RING1A/B). PRC1 represses gene expression through ubiquitination of H2A (H2AK119ub) (Bratzel et al., 2010; Calonje, 2014; Yang et al., 2013a). The PRC2 complex includes histone methyltransferases such as *CURLY LEAF* (*CLF*) and *SWINGER* (*SWN*) and promotes H3 trimethylation (H3K27me3) (Chanvivattana et al., 2004; Goodrich et al., 1997).

We have previously found that H3K27me3 increases at *MIR156A/C* in a PRC2-dependent manner during juvenile development, and that vegetative phase change is delayed in *swn* mutants (Xu et al., 2016b). The temporal deposition of H3K27me3 is accompanied by depletion of the antagonistic H3K27ac mark that is associated with active transcription. miR156 accumulation is also repressed by PRC1, as *atbmi1a/b* mutants exhibit delayed vegetative phase change (Pico et al., 2015). In addition, we have found that accumulation of the active histone mark H3K4me3 decreases at *MIR156A/C* during vegetative development (Xu et al., 2018).

The findings that H3K27me3 replaces H3K27ac and H3K4me3 at *MIR156A/C* over time, and that PRC1/PRC2-activity promotes vegetative phase change, led us to propose that the temporal dynamics of miR156 accumulation are coordinated by antagonistic patterns of active (H3K27ac, H3K4me3) and repressive (H3K27me3)

histone modifications (Xu et al., 2018, 2016b). In this model the stochastic removal of H3K27ac/H3K4me3 facilitates the deposition of H3K27me3 and the gradual epigenetic silencing of miR156. Similar mechanisms have been reported to function at other developmental transitions (Yang et al., 2014). For example, during flowering, H3K27 deacetylation is a pre-requisite for PRC2-mediated H3K27me3 deposition at *FLOWERING LOCUS C* (*FLC*) (Zeng et al., 2020), and during seed maturation, PRC1 promotes the exchange of H3K4me3 for H3K27me3 at *DELAY OF GERMINATION1* (*DOG1*) and *ABSCISIC ACID INSENSITIVE3* (*ABI3*) (Molitor et al., 2014).

Although there is good evidence that *MIR156A/C* are epigenetically silenced during vegetative development, how this mechanism is regulated temporally remains unknown. *VIVIPAROUS/ABI3-LIKE* (*VAL*) genes are excellent candidates for temporal effectors in this model. *VAL* genes encode B3 domain transcription factors that are closely related to the *ABI3/FUSCA3* (*FUS3*)/*LEAFY COYTLEDON2* (*LEC2*) clade of embryogenesis regulators. There are three *VAL* genes in *Arabidopsis*, of which *VAL1* and *VAL2* (also known as *HSI2* and *HSL2* respectively) are the most functionally important (Suzuki et al., 2007). VAL proteins repress their targets by binding to 6 base pair RY-sequence motifs (CATGCA) via their B3 domain (Chen et al., 2018, 2020; Guo et al., 2013; Jing et al., 2019; Qüesta et al., 2016; Suzuki et al., 1997; Yuan et al., 2016).

A number of observations suggest that *VAL* genes might provide the temporal information that coordinates vegetative phase change: 1) *VAL* genes regulate other developmental transitions, i.e. seed maturation (Suzuki et al., 2007; Yang et al., 2013a) and flowering (Qüesta et al., 2016; Yuan et al., 2016); 2) *MIR156A/C* expression is

elevated in *val1/2* mutants (Pico et al., 2015); 3) VAL1/2 physically interact with several histone deacetylases (*HDA6/9/19*) (Chhun et al., 2016; Qüesta et al., 2016; Zeng et al., 2020; Zhou et al., 2013); and 4) *VAL* genes promote PRC1 and PRC2-binding (Chen et al., 2018; Pico et al., 2015; Qüesta et al., 2016; Yuan et al., 2020, 2016)

In this study we investigated whether *VAL* genes function as temporal regulators of vegetative phase change. We report that reduced *VAL* activity significantly delays the timing of vegetative phase change through both miR156-dependent and independent mechanisms. We find that the temporal decline in miR156 expression is remarkably robust and is insensitive to loss of *VAL* function, inhibition of VAL1-binding and the combined loss of *VAL1* and PRC2 components. Finally, we show that the effects of *VAL1* on the timing of vegetative phase cannot be explained by temporal changes in its interactions with other proteins.

Results

VAL genes promote vegetative phase change

To investigate the role of *VAL* genes in vegetative phase change, we exploited a novel mutant we identified in an ethyl methanesulfonate screen for plants exhibiting prolonged juvenile development. Mapping-by-sequencing revealed a substitution at the *VAL1* locus, resulting in the conversion of a highly conserved arginine residue to a cysteine in the N-arm of the VAL1 B3 DNA-binding domain (Supplementary file 1A). This arginine residue is critical for VAL1 binding to target RY-motifs (Sasnauskas et al., 2018). The mutation in *VAL1* was confirmed to be the cause of the late juvenile phenotype by its failure to complement the null *val1-2* T-DNA insertion allele, and by the ability of the

VAL1 genomic sequence to rescue this phenotype (Supplementary file 1B,C). Unlike *val1-2*, the novel *val1* allele is semi-dominant, and delays vegetative phase change when heterozygous (Supplementary file 1D). We therefore named this new allele *val1-5(sd)*, consistent with the nomenclature of existing *val1* alleles (Veerappan et al., 2012).

Both *val1-5(sd)* and *val1-2* exhibit delayed vegetative phase change, with *val1-5(sd)* having a stronger effect on the timing of abaxial trichome production than *val1-2* (Supplementary file 1B). As *VAL1* functions redundantly with *VAL2* to regulate other developmental transitions (Qüesta et al., 2016; Suzuki et al., 2007; Tsukagoshi et al., 2007; Yuan et al., 2016), we tested the effects of *val1; val2* double mutants on vegetative phase change. Previous analyses of *VAL* gene function have utilized *val1-2; val2-1* and *val1-2; val2-3* double mutants. However, seedling development is so strongly perturbed in *val1-2; val2-1* and *val1-2; val2-3* plants (Suzuki et al., 2007; Tsukagoshi et al., 2007; Yang et al., 2013a; Yuan et al., 2020) that analyses of vegetative growth is problematic in these backgrounds. Therefore, we generated new *val1; val2* combinations using *val2-3* and a previously uncharacterized T-DNA insertion allele we named *val2-4* (Figure 1A). Consistent with previous studies (Suzuki et al., 2007; Tsukagoshi et al., 2007; Yuan et al., 2016), *val2* single mutants had no discernible effect on vegetative phase change (Figure 1B, Supplementary file 1E). However, loss of *VAL2* activity enhanced the phenotypes of *val1-2* and *val1-5(sd)*. *val1-2; val2-4* and *val1-5(sd); val2-3* both exhibited delayed abaxial trichome production relative to *val1-2* and *val1-5(sd)*, respectively (Figure 1C). *val1-5(sd)*; *val2-3* flowered significantly later than *val1-5(sd)* (Figure 1D) and *val1-2; val2-4* produced leaves that were significantly more juvenile in shape (i.e. rounder) than *val1-2* (Figure 1E). Neither double mutant

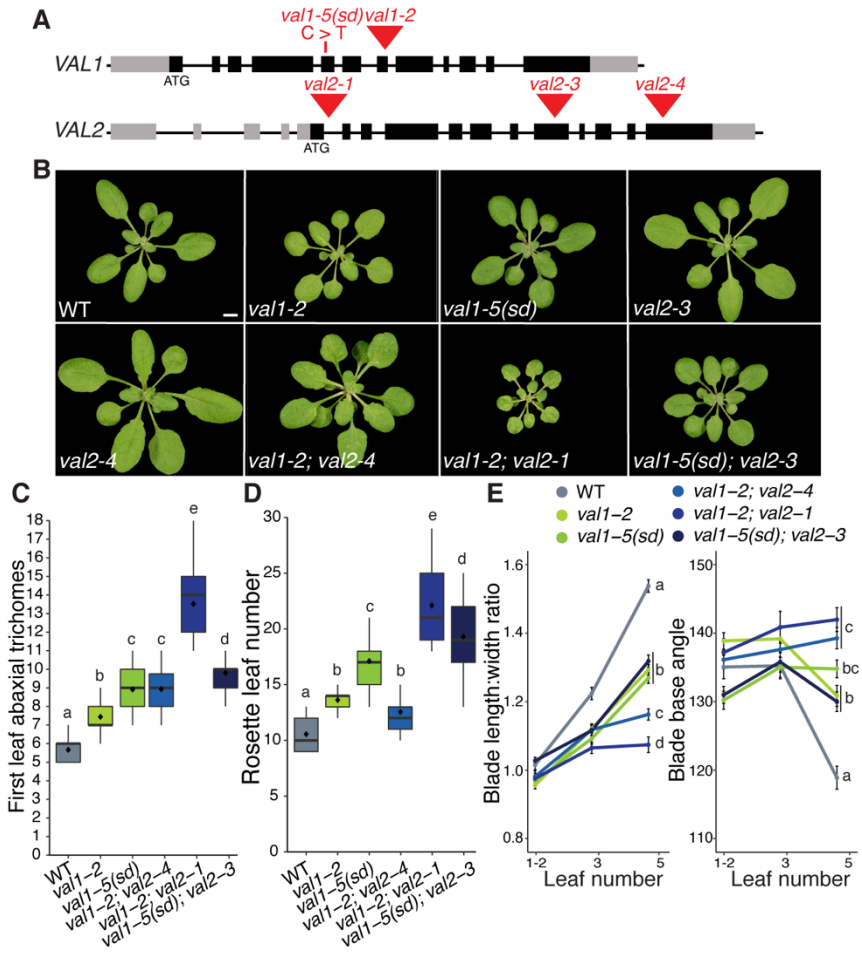

155 **Figure 1. *VAL* genes redundantly regulate vegetative phase change**

156 (A) Schematic of *val1* and *val2* alleles used in this study – grey boxes represent
157 UTRs, black boxes represent exons, red triangles represent T-DNA insertions,
158 red line represents EMS-induced base substitution.
159 (B) Phenotypes at 21 DAG in LD conditions, scale bar = 5mm.
160 (C-E) Quantitative analysis of vegetative development. Statistically distinct genotypes
161 were identified by one-way ANOVA with *post hoc* Tukey multiple comparison test
162 (letters indicate statistically distinct groups $P < 0.05$; for (E) comparisons were
163 made at leaf 5), all plants grown in LD. (C,D) Boxes display the interquartile
164 range (IQR) (boxes), median (lines) and values beyond 1.5*IQR (whiskers);
165 mean values are marked by ◆. (E) Colored lines represent the mean and black
166 bars the SEM. Sample sizes (C, D) 21-46, (E) 13-46.
167

combination was as phenotypically severe as *val1-2; val2-1* (Figure 1C-E). The weaker phenotype of *val1-5(sd); val2-3* than *val1-2; val2-3* (Yang et al., 2013a; Yuan et al., 2020) suggests that the semi-dominant phenotype of *val1-5(sd)* is mediated by interaction with *VAL2*. Importantly, the rate of germination was higher in *val1-2; val2-4* and *val1-5(sd); val2-3* relative to existing *val1; val2* double mutants. *val1-2; val2-4* and *val1-5(sd); val2-3* thus provide a balance between phenotypic strength and experimental viability and are useful tools for investigating the role of *VAL* genes in developmental timing.

VAL genes function predominantly as quantitative – rather than temporal – regulators of miR156 expression

Vegetative phase change results from a temporal decline in miR156 expression (Wu and Poethig, 2006). A previous analysis of *val1-2; val2-1* revealed elevated expression of *MIR156A/C* at a single time point (Pico et al., 2015). To determine whether the delay in vegetative phase change we observed in *val* mutants is associated with a general increase in the level of miR156, or with a delay in the decline in this miRNA, we quantified miR156 expression in the shoot apex and in isolated leaf primordia at different times in shoot development. The primary transcripts of *MIR156A* and *MIR156C* were expressed at similar levels, and exhibited a similar temporal expression pattern, in wild type, *val1-5(sd)* (Figure 2A,B) and *val1-2* shoot apices and leaf primordia (Supplementary file 2). However, the abundance of the mature miR156 miRNA transcript was significantly higher in *val1-5(sd)* leaf primordia than in wild type (Figure 2B), and it was also marginally higher in *val1-5(sd)* shoot apices than in wild type

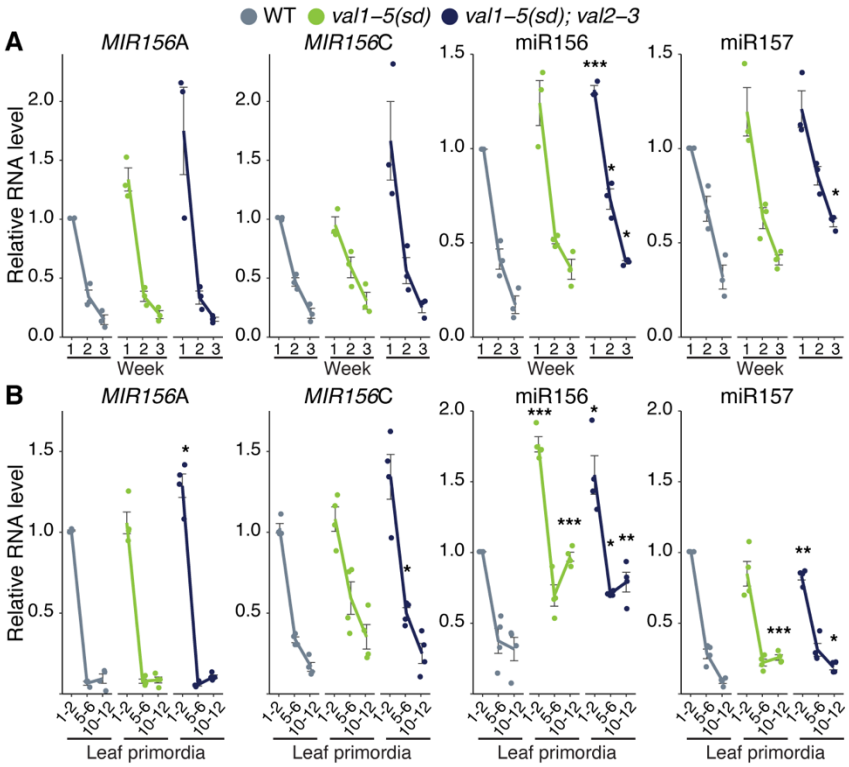

Figure 2. *VAL* genes function predominantly as quantitative regulators of miR156 expression

(A, B) qRT-PCR analyses of gene expression. (A) Shoot apices with leaf primordia (LP) ≥ 1mm removed at 1, 2 and 3 weeks. (B) Isolated LP 0.5-1mm in size. All plants were grown in SD conditions. Each data point represents a biological replicate and is the average of three technical replicates. Coloured lines represent the mean and black bars mean±s.e.m. Asterisks represent significant differences between WT and *val* mutants at the same time point, calculated by an unpaired two-tailed *t*-test with a Bonferroni correction for multiple comparisons (* $P < 0.025$; ** $P < 0.005$; *** $P < 0.0005$).

(Figure 2A). The *val1-5(sd); val2-3* (Figure 2A,B) and *val1-2; val2-1* (Supplementary file 2) double mutants had stronger effects on *MIR156A* and *MIR156C* expression than the respective *val1* single mutants, suggesting that *VAL1* and *VAL2* function redundantly to repress *MIR156A* and *MIR156C* transcription. Mature miR156 was elevated throughout development in both the shoot apices (Figure 2A) and the leaf primordia (Figure 2B) of *val1-5(sd); val2-3* double mutants. Loss of *VAL* activity also produced a slight increase in miR157 levels (Figure 2A,B, Supplementary file 2). Although *val1-5(sd); val2-3* increased the abundance of miR156/miR157, it had only a minor effect on the temporal expression patterns of these miRNAs. For example, miR156 expression decreased 2.36-fold between 1W and 2W and 2.31-fold between 2W and 3W in wild type plants, but decreased 1.77 and 1.82-fold between the same time points in *val1-5(sd); val2-3* plants (Figure 2A). Taken together, these data suggest that *VAL* genes function primarily as general, rather than temporal, regulators of miR156 expression.

***VAL* genes coordinate PRC1 and PRC2 recruitment at *MIR156* loci**

We have previously demonstrated that the temporal decline in *MIR156A* and *MIR156C* expression is associated with PRC2-dependent and progressive deposition of H3K27me3 at these loci (Xu et al., 2016b). To determine if *VAL* genes contribute to this process, we examined PRC2 activity in the *val1-5(sd); val2-3* double mutant. As previously reported (Xu et al., 2016b), H3K27me3 levels increased at the *MIR156A* and *MIR156C* loci during vegetative development in wild type plants (Figure 3A,B). Although there was no difference in the temporal pattern of H3K27me3 deposition at *MIR156A* in

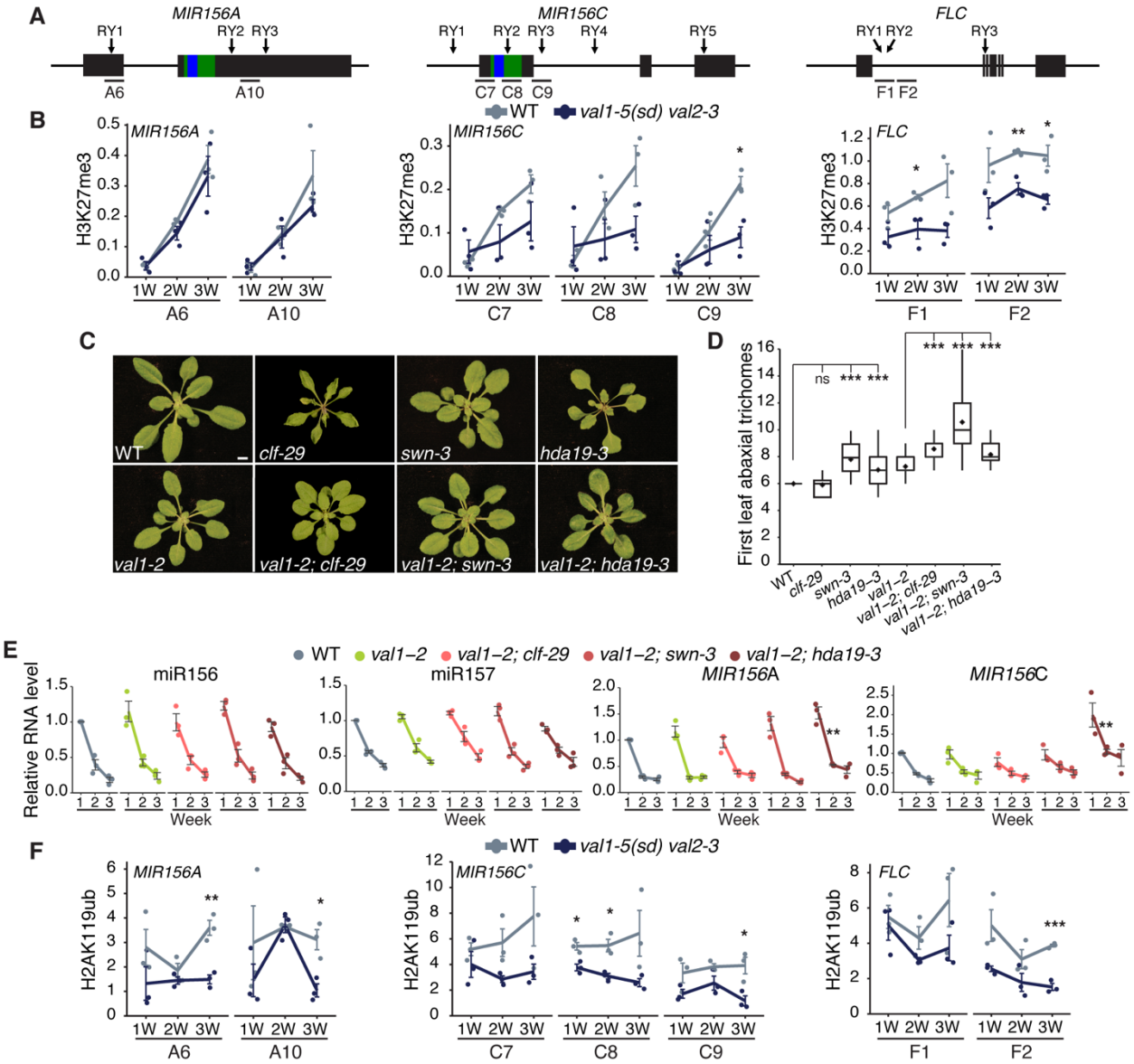

Figure 3. *VAL* genes regulate miR156 activity via-PRC2 and PRC1

(A) Schematics of the primer locations used for ChIP-qPCR. Blue and green bars represent sequences encoding the mature miRNA and miRNA hairpin respectively.

(B) Temporal analysis of H3K27me3 by ChIP-qPCR. Each data point represents a biological replicate and is the average of three technical replicates. Lines represent the mean, bars represent the mean±s.e.m., asterisks represent significant differences between WT and *val1-5(sd); val2-3* at the same time point, calculated by an unpaired two-tailed *t*-test (* $P < 0.05$; ** $P < 0.01$; *** $P < 0.001$). H3K2me3 values are relative to H3 and normalised to *STM* as an internal control. Plants were grown in SD conditions.

(C, D) Phenotypes in LD. (D) Photographs taken at 21DAG, scale bar = 5mm. (E) Asterisks represent significant differences to either WT or *val1-2*, calculated by unpaired two-tailed *t*-test with Bonferroni correction for multiple comparisons (*** $P < 0.00033$). Sample size 22-46.

(E) qRT-PCR analyses of gene expression in shoot apices with LP ≥ 1mm removed at 1, 2 and 3 weeks. Each data point represents a biological replicated and is the average of three technical replicates. Coloured lines represent the mean and black bars represent the mean±s.e.m. Asterisks represent significant differences between *val1-2* and *val1-2; clf-29/val1-2; swn-3/val1-2; hda19-3* at the same time point, calculated by unpaired two-tailed *t*-test with Bonferroni correction for multiple comparisons (** $P < 0.0033$). Plants were grown in SD conditions.

(F) Temporal analysis of H2AK119ub by ChIP-qPCR, values are relative to input and normalised to *ACT7* as an internal control. See (B) for details.

val1-5(sd); val2-3, the rate of H3K27me3 deposition at *MIR156C* was significantly slower in this double mutant (Figure 3B). These results are consistent with a recent genome-wide study that revealed a decrease in H3K27me3 levels at *MIR156C*, but not *MIR156A*, in *val1-2; val2-3* plants (Yuan et al., 2020). As a control, we measured H3K27me3 deposition at the floral regulator *FLC.* In the absence of vernalization, we observed no change in the level of H3K27me3 during vegetative development in wild type plants (Figure 3B). However, consistent with previous reports (Qüesta et al., 2016; Yuan et al., 2016), there was a significant decrease in H3K27me3 at *FLC* in *val1-5(sd); val2-3*.

VAL1 is thought to act by recruiting PRC1 which, in turn, promotes the activity of PRC2 (Baile et al., 2020; Calonje, 2014; Zhou et al., 2017). As a genetic test of this hypothesis, we examined the interaction between *val1-2* and *clf-29* and *swn-3,* loss-of-function mutations in the functionally redundant genes that encode the histone methyltransferase activity of PRC2. As we have shown previously (Xu et al., 2016b), *swn-3* had a larger effect on the timing of vegetative phase change than *clf-29* (Figure 3C,D). Consistent with the hypothesis that *VAL1* regulates vegetative phase via its effect on PRC2 activity, *clf-29* and *swn-3* interacted synergistically with *val1-2,* in that the double mutants had a much more severe vegetative phase change phenotype than the single mutants (Figure 3C,D). Notably, *val1-2* suppressed the curling leaf phenotype of *clf-29* (Figure 3C), presumably because it enhances *FLC* expression (Lopez-Vernaza et al., 2012). We also examined the interaction between *val1-2* and *hda19-3*, a putative null allele of the histone deacetylase HDA19. *hda19-3* is predicted to delay vegetative phase change because *HDA19* is required for PRC2-mediated repression (Zeng et al.,

2020), HDA19 physically interacts with VAL1 (Qüesta et al., 2016) and loss-of *HDA19* enhances H3K4me3 levels (Jang et al., 2011). As predicted, *hda19-3* produced abaxial trichomes significantly later than wild type (Figure 3D), and *val1-2; hda19-3* double mutants produced abaxial trichomes significantly later than either single mutant. Together, these results suggest that *val* mutations delay vegetative phase change by interfering with the activity of PRC2.

To determine whether the synergistic interaction between *clf-29, swn-3, hda19-3* and *val1-2* is due to enhanced miR156/miR157 expression, we quantified expression of the mature miR156 and miR157 miRNAs, and the primary *MIR156A* and *MIR156C* transcripts, in these mutant backgrounds. The overall level and expression pattern of the mature miR156/miR157 transcripts were not affected by *val1-2*, or by *val1-2; clf-29*, *val1-2; swn-3*, and *val1-2; hda19-3* double mutants (Figure 3E). However, *pri-MIR156A* and *pri-MIR156C* transcripts were significantly elevated in *val1-2; hda19-3,* although the rate of decline in the expression of these transcripts was normal. The lack of correlation between the expression of miR156 and the level of *pri-MIR156A* and *pri-MIR156C* is surprising given that these loci are the major sources of miR156. One possibility is that the miRNA processing pathway is compensating for elevated levels of the primary transcripts. In any case, these results suggest that *VAL* genes temporally regulate the deposition of H3K27me3 at specific *MIR156* loci, but are not necessary for the temporal decline in miR156 expression.

VAL genes also repress gene expression by promoting H2AK119ub deposition via recruitment of PRC1 (Yang et al., 2013a). Unlike H3K27me3 (Figure 3B) (Xu et al., 2016b), we found no evidence that H2AK119ub increases over time at *MIR156A* and

MIR156C (Figure 3F). However, we did find that *val1-5(sd); val2-3* had significantly lower levels of H2AK119ub than wild type plants. This effect was observed throughout development at *MIR156C*, but seemed to be limited to later in development at *MIR156A*. Importantly, *val1-5(sd); val2-3* had significantly reduced levels of H2AK119ub at *MIR156C* one week after planting, which is before a difference in H3K27me3 is detectable at this locus (Figure 3B). *val1-5(sd); val2-3* also had reduced levels of H2AK119ub at *FLC* (Figure 3F).

VAL1 regulates vegetative phase change via miR156-dependent and miR156-independent mechanisms

To investigate whether the effects of *val1-5(sd); val2-3* on the chromatin state of *MIR156A/C* are due to a direct regulatory interaction, we carried out chromatin-immunoprecipitation qPCR using an HA-tagged version of VAL1 (Qüesta et al., 2016). Confirming the results of a recent ChIP-seq study (Yuan et al., 2020), we found VAL1-binding at specific locations within both the *MIR156A* and *MIR156C* loci (Figure 4A,B, Supplementary file 3). The affinity of VAL1 for *MIR156A/C* appeared consistent throughout vegetative development. VAL1/2 bind to RY-sequence motifs, of which there are multiple copies in both *MIR156A* and *MIR156C* (Figure 4A). To determine if these RY-sites are required for the regulation of vegetative phase change, we mutated 5 RY-sites in *MIR156C* individually and in combination. We selected *MIR156C* because it is more sensitive to *VAL* activity than *MIR156A* (Figure 2,3, Supplementary file 2). A C>T substitution that eliminates VAL1 binding (Sasnauskas et al., 2018) was introduced in one or all of these sites in a genomic construct of *MIR156C*. Wild type and mutant

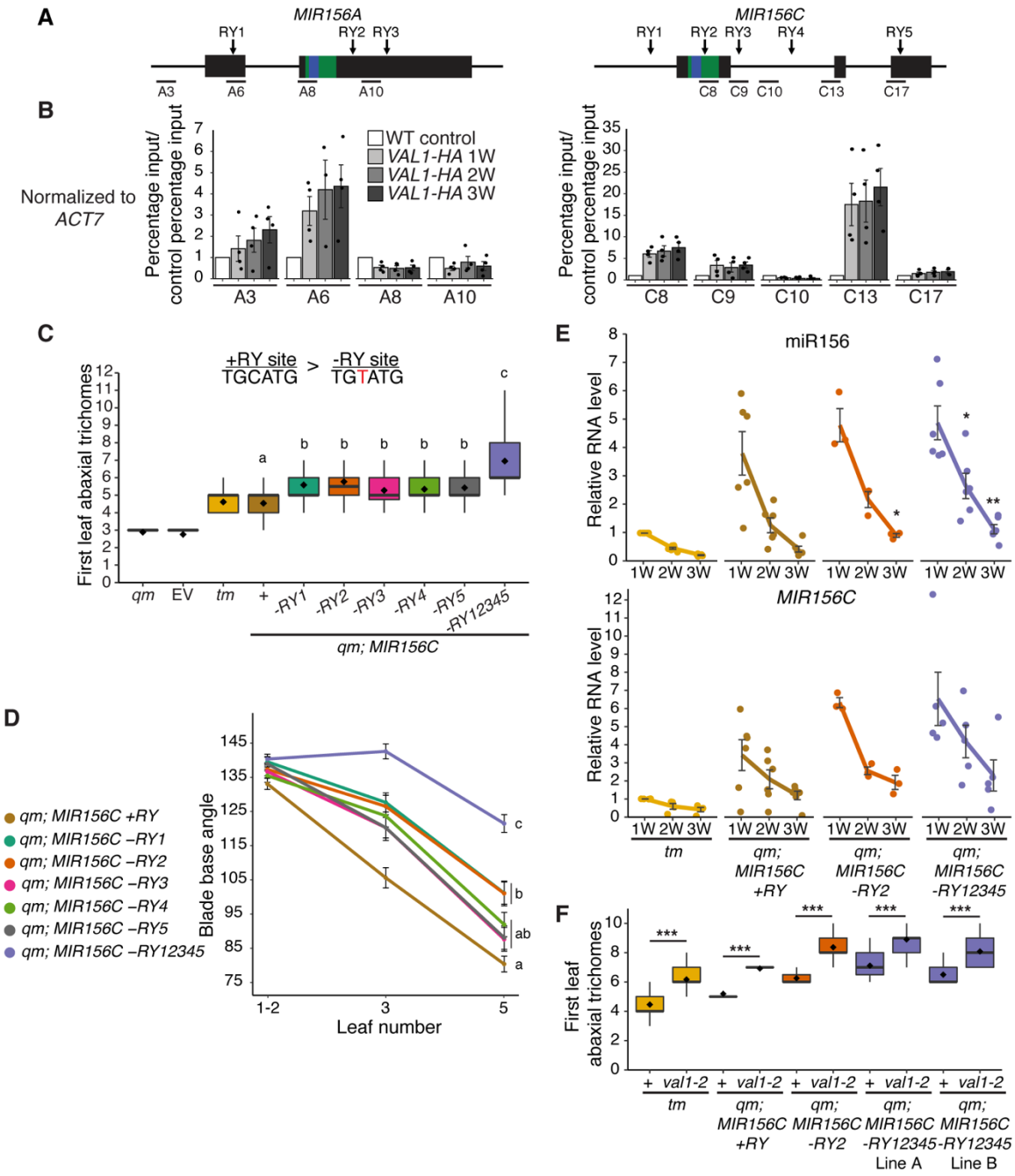

Figure 4. Loss of RY VAL-binding motifs at the *MIR156C* locus delays vegetative phase change

(A) Schematic depicting the location of primers used for ChIP-qPCR, the sequences encoding the miR156 hairpin and mature miRNA are coloured green and blue respectively.

(B) Anti-HA ChIP-qPCR of WT Col control plants at 2W and *VAL1::VAL1-HA; val1-2; FRI-Sf2* plants at 1, 2 and 3W of growth. The data is presented as percentage input normalized to *ACT7* and is displayed relative to WT. Each data point represents a biological replicate and is the average of three technical replicates, bars represent the mean and error bars the mean±s.e.m.

(C, D) Phenotypes of T1 plants transformed with *MIR156C* RY variants. Statistically distinct genotypes were identified by one-way ANOVA with *post hoc* Tukey multiple comparison test (letters indicate statistically distinct groups $P < 0.05$; comparison in (C) made at leaf 5). *qm = mir156a mir156c mir157a mir157c quadruple mutant, tm = mir156a mir157a mir157c triple mutant,* EV = empty vector. (C) Colored lines represent the mean and black bars the mean±s.e.m. Sample size (B) 26-52, (C) 37-51.

(E) qRT-PCR analyses of gene expression in shoot apices with LP ≥ 1mm removed at 1, 2 and 3 weeks. Each data point represents an independent homozygous T3 line and is the average of three technical replicates. Colored lines represent the mean and black bars the mean±s.e.m. Asterisks represent significant differences between *qm; MIR156C* and *qm; MIR156C -RY* lines at the same time point, calculated by an unpaired two-tailed *t*-test with a Bonferroni correction for multiple comparisons (* $P < 0.025$, ** $P < 0.005$).

(F) Genetic interaction between *val1-2* and *MIR156C* RY deletions. Asterisks represent significant differences between plants with wild type or null *VAL1* alleles calculated by an unpaired two-tailed *t*-test (*** $P < 0.001$). Sample size 24-36. Phenotyping analyses were carried out in LD conditions, gene expression and ChIP analyses were carried out in SD conditions.

353 constructs were then transformed into a *mir156a; mir156c; mir157a; mir157c quadruple*
354 *mutant* (*qm*) background. We chose this background because endogenous
355 miR156/miR157 activity has been largely eliminated and it is therefore sensitive to small
356 changes in the level of miR156 (He et al., 2018). Plants transformed with a wild type
357 *MIR156C* construct (+*RY*) produced leaves with abaxial trichomes at the same node as
358 the *mir156a; mir157a; mir157c triple mutant tm* (Figure 4C). *tm* has an endogenous
359 copy of *MIR156C*, confirming that the transgenic *MIR156C* sequence is fully functional.
360 Deletion of individual RY-sites produced a significant delay in the timing of abaxial
361 trichome production relative to *MIR156C +RY*, and deletion of all 5 RY-sites produced a
362 more significant delay than deletion of any single site (Figure 4C). A similar result was
363 obtained in the case of the angle of the leaf base (Figure 4D). These results
364 demonstrate that all five RY-sites are important for the expression of *MIR156C*, and that
365 they function additively. Individual RY-sites have also been shown to interact additively
366 to repress the VAL1-PRC2 targets *FLC* and *DOG1* (Chen et al., 2020; Yuan et al.,
367 2016).

368 To determine if these phenotypic effects are due to altered *MIR156C* expression,
369 we quantified miR156 levels in *MIR156C +RY, MIR156C -RY2* and *MIR156C -RY12345*
370 plants. *MIR156C -RY2* was selected because it has a marginally stronger effect than
371 other individual -RY deletions (Figure 4C,D). Although there was considerable variation
372 in miR156 levels between independent transgenic lines, *MIR156C -RY2* and *MIR156C -*
373 *RY12345* plants had significantly more miR156 than plants transformed with *MIR156C*
374 *+RY* (Figure 4E, Supplementary file 4). However, the temporal expression pattern of
375 *MIR156C* was identical in -*RY* and +*RY* plants.

To establish whether the effects of RY-deletion are *VAL1*-dependent, we crossed *val1-2* into the *qm; MIR156C +/-RY* lines. If the delay in vegetative phase change in *MIR156C -RY* lines is a consequence of reduced VAL1 binding, *val1-2* should have less effect in *MIR156C -RY* lines than in *MIR156C +RY* lines or the *tm*, in which RY sites are intact. Surprisingly, we found that loss-of *VAL1* significantly delayed abaxial trichome production in *MIR156C -RY* as well as *MIR156C +RY* and *tm* plants (Figure 4F). It is possible that *MIR156C* RY-sites are bound by other B3 domain transcription factors. However, RY-binding is restricted to the *ABI3/FUS3/LEC2* and *VAL* clade of B3 domain genes (Kagaya et al., 1999; Sasnauskas et al., 2018; Yuan et al., 2016). The expression of *ABI3/FUS3/LEC2* is largely restricted to seed development (Carbonero et al., 2017) and therefore these genes are unlikely to regulate vegetative shoot identity. Moreover, FUS3 and ABI3 directly promote the expression of *MIR156C* (Tian et al., 2020; Wang and Perry, 2013). A role for these genes in the regulation of *MIR156C* post-germination is thus inconsistent with the juvenilized phenotype and elevated miR156 expression we found in *MIR156C -RY* plants. (Figure 4C-E). With regard to the potential effects of other *VAL* genes, we observed no vegetative phase change phenotype in *val2* single mutants (Figure 1B, Supplementary file 1E) and *VAL3* has limited expression and functionality relative to *VAL1* and *VAL2* (Suzuki et al., 2007). Alternatively, this result suggests that *VAL1* may regulate vegetative phase change through both miR156-dependent and miR156-independent mechanisms. This interpretation is supported by the observation that loss-of *VAL1* and PRC2-components strongly delayed vegetative phase change but had only minor effects on miR156 expression (Figure 3C-E).

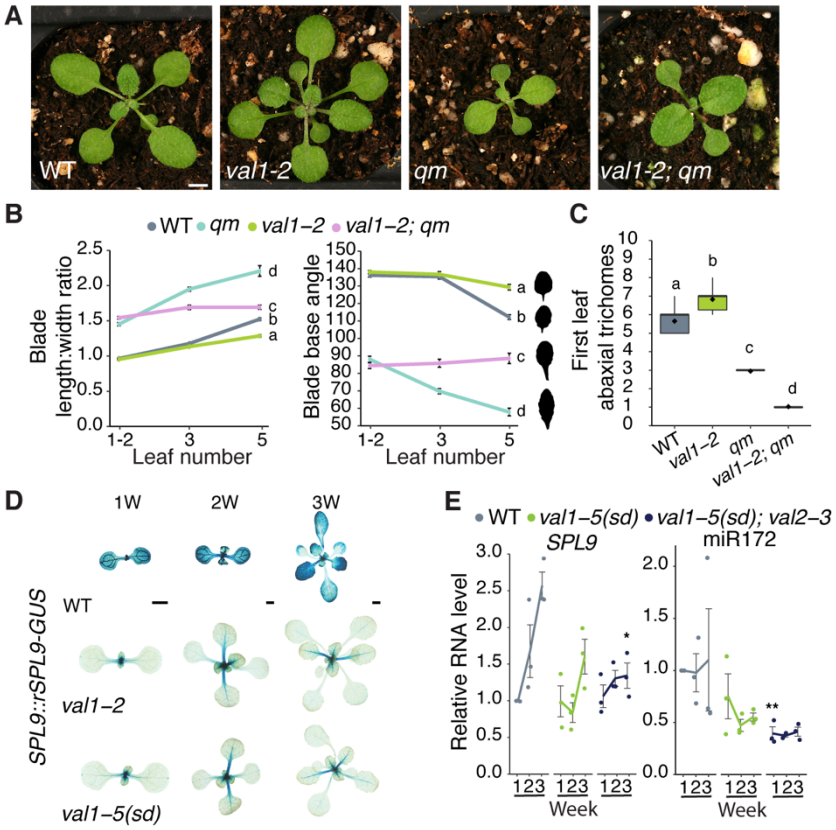

Figure 5. *VAL1* regulates vegetative phase change by miR156-dependent and independent mechanisms

(A-C) Phenotypes of *val1-2* and *mir156a mir156c mir157a mir157c quadruple mutant* lines. (A) Photographs taken at 17 DAG. Scale bar = 1mm. (B, C) Statistically distinct genotypes were identified by one-way ANOVA with *post hoc* Tukey multiple comparison test (letters indicate statistically distinct groups $P < 0.05$; (B) comparisons made at leaf 5). Bars represent the mean±s.e.m. Sample size (B) 17-60, (C) 18-36. Silhouettes in B show representative leaf 5 shapes.

(D) Expression of a miR156-resistant (*rSPL9*) reporter construct in WT, *val1-2* and *val1-5(sd)* backgrounds. Scale bars = 1mm.

(E) qRT-PCR analysis of gene expression in shoot apices with LP ≥ 1mm removed at 1, 2 and 3 weeks. Each data point represents a biological replicate and is the average of three technical replicates. Coloured lines represent the mean and gray bars represent the mean±s.e.m. Asterisk represents significant difference between WT and *val* mutant lines at the same time point, calculated by an unpaired two-tailed *t*-test with a Bonferroni correction (* $P < 0.025$; ** $P < 0.005$). All phenotypic analyses were carried out in LD conditions, the gene expression analysis was carried out in SD conditions.

To test this hypothesis, we introgressed *val1-2* into the *qm* genetic background, which has very low levels of miR156/miR157 (He et al., 2018). Although the gross morphology (Figure 5A) of *val1-2*; *qm* seedlings was indistinguishable from that of *qm* plants, *val1-2* partially suppressed the effect of the *qm* genotype on the morphology of leaves 3 and 5 (Figure 5B). This confirms that *VAL1* functions through a miR156/miR157-independent mechanism to regulate vegetative phase change. Surprisingly, a survey of abaxial trichome production revealed that *val1-2* enhanced this aspect of the precocious *qm* phenotype (Figure 5C). This result can be explained given that reduced histone deacetylation in a *toe* loss-of-function background accelerates abaxial trichome formation (Wang et al., 2019), that *SPL* genes repress *TOE* activity (Wu et al., 2009), and that *VAL* genes promote histone deacetylation (Zeng et al., 2020; Zhou et al., 2013).

To determine if *VAL1* regulates *SPL* gene expression independently of miR156, we crossed a miR156-resistant (*rSPL9*) *SPL9::rSPL9-GUS* reporter construct into *val1* genetic backgrounds. The expression of this reporter was visibly and strongly suppressed by *val1-2* and *val1-5(sd*) (Figure 5D), implying that miR156 is not required for the regulation of *SPL9* by *VAL1*. The transcript levels of *SPL9*, and its target miR172, were also decreased in *val* mutant plants (Figure 5E). However, it is difficult to know if this decrease is dependent or independent of miR156 because miR156 induces cleavage of the *SPL9* transcript (German et al., 2008; He et al., 2018; Ronemus et al., 2006).

VAL1/2 act as transcriptional repressors. As *SPL9* transcription decreases in *val* loss-of function mutants it is therefore unlikely that VAL1/2 regulate *SPL9* directly. To

test this prediction, we quantified H2AK119ub and H3K27me3 at *SPL9.* Consistent with previous studies, we found high levels of H2AK119ub but negligible H3K27me3 at *SPL9* (Supplementary file 5) (Li et al., 2017; Zhou et al., 2017). We also found no difference in the abundance of these modifications in wild type and *val1-5(sd); val2-3* plants. Taken together these results suggest that, in addition to repressing *SPL9* via their effect on miR156 levels, VAL1/2 repress *SPL9* indirectly through one or more miR156-independent mechanisms. The observation that *val1-5(sd); val2-3* has no effect on H2AK119ub at *SPL9* also suggests that *VAL1/2* are not universally required for PRC1-activity.

The effects of *VAL1* on developmental timing may be partly explained by its expression pattern

Our results show that *VAL* genes control the timing of vegetative phase change (Figure 1C,E), and have subtle effects on the expression pattern of miR156 during vegetative development (Figure 2, Supplementary file 2). To determine if these effects are attributable to changes in the expression level of *VAL1*, we measured the abundance of *VAL1* transcript levels during vegetative growth. We observed a small but significant increase in *VAL1* transcripts in shoot apices between 2 and 3 weeks of growth (Figure 6A) but there was no significant change in *VAL1* levels in leaf primordia (Figure 6B). To further investigate *VAL1* expression over time, we generated a *VAL1* transcriptional reporter by fusing a 2.3kb sequence containing the *VAL1* promoter and 5' UTR, and a 2kb sequence containing the *VAL1* 3'UTR and terminator, to the GUS coding sequence (*VAL1::GUS-VAL1 3' UTR)*. We generated a *VAL1* translational fusion by inserting a

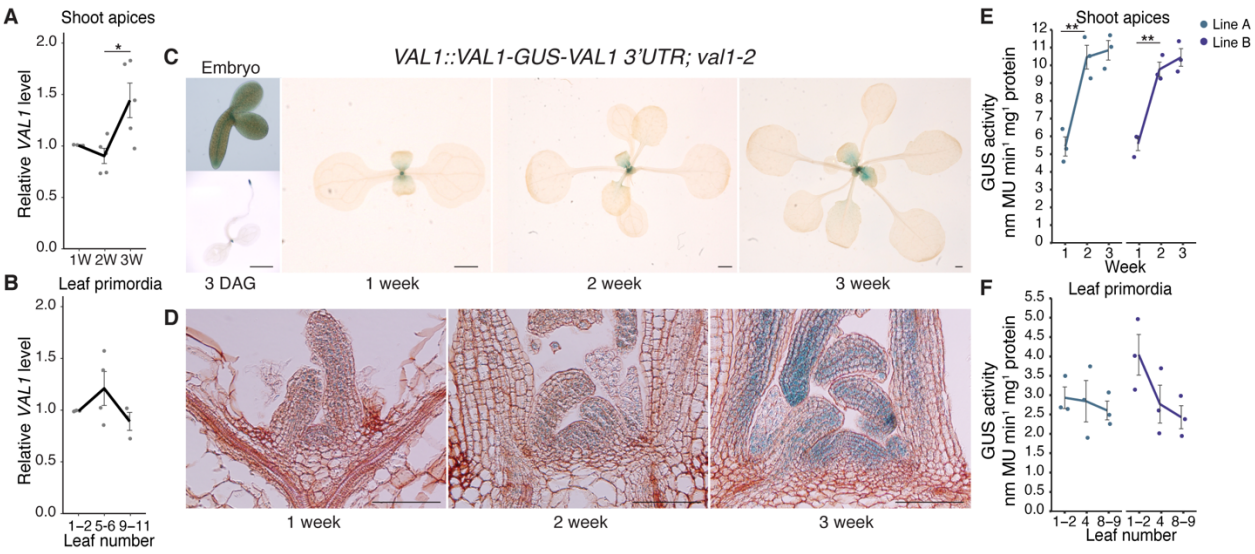

Figure 6. *VAL1* is expressed throughout vegetative development

(A, B) qRT-PCR analyses of gene expression. (A) Shoot apices with leaf primordia (LP) ≥ 1mm removed at 1, 2 and 3 weeks. (B) Isolated LP 0.5-1mm in size.

(C-F) Analyses of a *VAL1-GUS* translational fusion. (C) Expression in whole plants, scale bars = 1mm. (D) Expression in shoot apices following wax sectioning, scale bars = 0.1mm. (E, F) VAL1 levels quantified by MUG assay in two independent homozygous T3 lines. (A, B, E, F) Each data point represents a biological replicate and is the average of three technical replicates. Lines represent the mean and grey bars mean±s.e.m. Asterisks represent significant differences between two continuous time points, calculated by an unpaired two-tailed *t*-test (* $P < 0.05$; ** $P < 0.01$). All plants except the 3 DAG sample (C – long days) were grown in SD conditions.

3.8kb *VAL1* genomic sequence upstream of *GUS* in this construct (*VAL1::VAL1-GUS-VAL1 3'UTR*). Because the expression of the transcriptional fusion was consistently more diffuse, variable, and weaker than the expression of the translational fusion (Supplementary file 6), we used plants containing the translational fusion for subsequent studies.

During embryogenesis, the translational fusion was expressed in the root and shoot apical meristems and provasculature (Figure 6C, Supplementary file 6). Following germination, expression became restricted to the shoot and root apices and initiating lateral root primordia (Figure 6C, Supplementary file 6). Throughout the rest of shoot development, the translational fusion was expressed in the shoot apex and during the early stages of leaf development (Figure 6C). Histological inspection indicated that *VAL1* expression increases in the shoot apex during vegetative development. This was validated by a quantitative analysis of GUS expression, which demonstrated that VAL1 accumulates more strongly in the shoot apex than leaf primordia. Further, that VAL1 levels increase over time in the shoot apex but not in older leaf primordia (Figure 6E,F). Taken together, these data indicate that *VAL1* expression is restricted to apical meristems and the early stages of root and leaf development. Our data also indicate that *VAL1* expression increases during shoot development in very young leaf primordia, quickly declines to a uniform level as the leaf develops, and ceases before the leaf is fully expanded. However, the functional significance of increased VAL1 accumulation during vegetative development is unclear, as we did not detect a concomitant increase in VAL1-binding to *MIR156A/C* (Figure 4B, Supplementary file 3). Finally, the difference in the staining patterns and stability of our transcriptional and translational reporters

suggest that *cis*-regulatory elements within the *VAL1* coding sequence regulate the level and site of its expression.

VAL1 has previously been found to physically interact with VAL2, multiple PRC1 and PRC2 components, and the transcriptional repressor SAP18 (Chen et al., 2018, 2020; Chhun et al., 2016; Jing et al., 2019; Qüesta et al., 2016; Xie et al., 2018; Yang et al., 2013a; Yuan et al., 2016). However, these studies do not provide information about VAL1's *in planta* protein interactions over time. To determine whether VAL1 interacts with different proteins at different stages of vegetative development, we carried out a mass spectrometry analysis of proteins bound to HA-tagged VAL1 at 1, 2 and 3 weeks of growth. Immunoprecipitations were carried out on a *VAL1-HA; val1-2; FRI-Sf2* line, using a *val1-2; fri* line as a control. The difference in the *FRI* genotype of these lines is a consequence of the genotypes available at the time the experiments were performed and may have had an effect on our results.

ATBMI1A was significantly enriched in the combined experimental samples relative to the control samples (Figure 7A), which is consistent with a previous mass spectrometry analysis of proteins bound to VAL1-HA (Qüesta et al., 2016). We did not detect other proteins that have been identified by mass spectrometry in immunoprecipitation experiments with VAL1-HA. We also observed a highly significant enrichment of the chloroplast binding protein CRB. However, this is explained by the enrichment of CRB in the total proteome of the experimental versus control samples (Figure 7B). Comparisons of the proteins present in samples harvested from 1, 2 and 3 weeks old plants revealed that ATBMI1A was consistently among the most abundant proteins immunoprecipitated with VAL1-HA (Figure 7C-E). The abundance of ATBMI1A

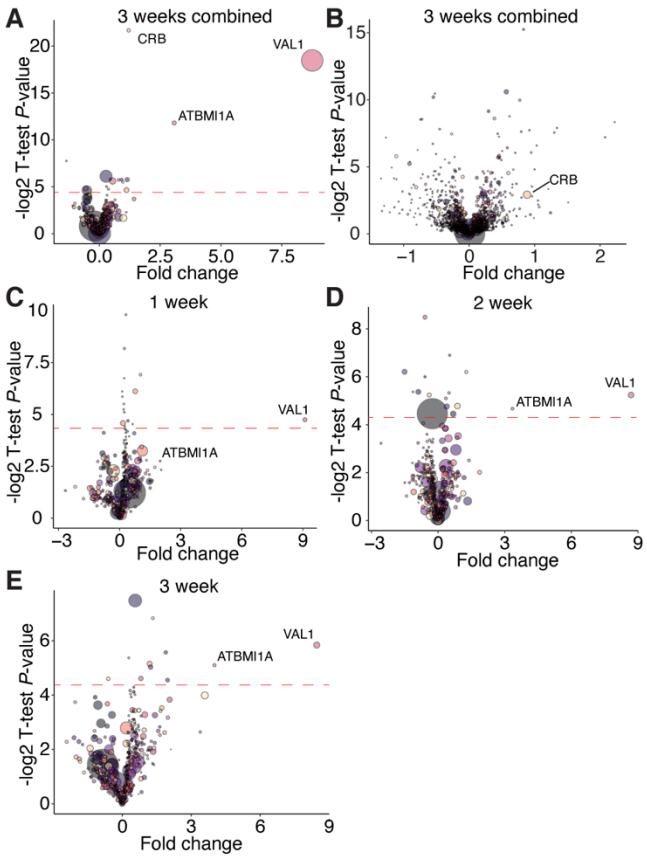

Figure 7. VAL1-protein interactions are consistent during vegetative development

(A-E) Protein enrichment calculated via mass spectrometry. Fold change represents the ratio of proteins purified from experimental (*VAL1-HA; val1-2; FRI-Sf2*) to control (*val1-2; fri*) samples, a t-test *P*-value is represented on the y-axis. Red dotted line indicates a *P*-value < 0.05 (resulting from the -log2 transformation of the actual p-value; proteins above the line have a significant enrichment). Each bubble represents an individual protein, the size or the bubble represents the protein abundance averaged across the experimental and control samples. (A, C-E) Proteins immunoprecipitated using an anti-HA antibody, (B) total proteome samples.

in the immunoprecipitated sample increased significantly from 1 week to 2 weeks, as indicated by both the increase in the fold change between experimental and control samples, and the statistical significance of the enrichment. This is probably a result of the increase in the abundance of VAL1 between 1 and 2 weeks (Figure 6D,E), a result which was confirmed by the increasing abundance of VAL1 in the immunoprecipitated samples from different time points (Figure 7C-E). The parallel changes in the abundance of VAL1-HA and ATBMI1A, and the absence of any major change in the proteins associated with VAL1-HA in different samples, suggest that the binding partners of VAL1 do not change significantly during shoot development.

To investigate overall trends in protein accumulation during vegetative development we conducted a supervised clustering analysis of the *val1-2; VAL1-HA; FRI-Sf2* total proteome sample. We designed two clusters in which proteins either increased or decreased from 1 to 2 to 3 weeks of development (see Methods for details). The 50 proteins with the strongest and most consistent decreasing developmental trend were significantly enriched for Gene Ontology terms related to photosynthesis and carbon fixation (Supplementary file 7). In contrast, the 50 proteins with the highest increasing trend score were enriched for GO terms relating to water stress and translation. The finding that younger plants invest more resources in photosynthesis is consistent with a transcriptomic analysis of vegetative development in maize (Beydler et al., 2016), and the enhanced photosynthetic capacity of juvenile plants at low light levels (Lawrence et al., 2020).

Discussion

Plant life cycles are characterized by transitions between distinct developmental phases. *VAL* genes have previously been shown to promote the switch from embryogenesis to seed maturation (Suzuki et al., 2007; Yang et al., 2013a), and from vegetative to reproductive growth (Qüesta et al., 2016; Yuan et al., 2016). The results presented here demonstrate that *VAL1* and *VAL2* also regulate the intervening transition from juvenile to adult stages of vegetative growth. *VAL* genes thus function as a regulatory hub that coordinates developmental transitions throughout plant life cycles.

Regulation of miR156 expression by *VAL1/2*

Vegetative phase change is promoted by a temporal decline in miR156/miR157 expression (Wu and Poethig, 2006). When the level of miR156/miR157 falls below a specific threshold, the de-repression of *SPL* genes initiates a switch to adult identity. Previous work has shown that – with the exception of *SPL3* – the increase in *SPL* transcript levels during development is entirely attributable to post-transcriptional regulation by miR156/miR157 (He et al., 2018). Factors that control the timing of vegetative phase change can therefore act in three ways: 1) by modifying the rate of decline in miR156; 2) by constitutively increasing or decreasing the level of miR156; and 3) by constitutively increasing or decreasing the rate of transcription of *SPL* genes. Our results suggest that *VAL1* and *VAL2* regulate vegetative phase change both by constitutively decreasing the level of miR156 and by repressing *SPL* gene expression independently of miR156.

Evidence that *VAL1/VAL2* constitutively regulate the level of miR156 was provided by the phenotype of plants deficient for *VAL1* and *VAL2*, VAL1-DNA binding

patterns and from the phenotype of plants expressing a *MIR156C* transgene lacking VAL-binding sites. We found that although *VAL1* expression increases in the shoot apex as plants develop, *val1; val2* double mutants displayed only a slight decrease in the rate at which miR156 declines. Instead, *val1; val2* double mutants exhibited a significant increase in the level of miR156 at every stage of vegetative development we examined. Consistent with this result, *mir156a; mir157a; mir157c* triple mutants transformed with a *MIR156C* transgene lacking VAL-binding sites had elevated levels of miR156 relative to the wild type *MIR156C* control, but displayed the same temporal decrease in miR156 as control plants.

We have proposed that the decrease in *MIR156A/C* expression during shoot development may be attributable to the stochastic replacement of H3K27ac and H3K4me3 by H3K27me3 (Xu et al., 2018, 2016b). The observation that the increase in miR156 expression in *val1; val2* is associated with a decrease in the level of H3K27me3 at *MIR156C* supports this hypothesis, in that it shows that H3K27me3 is associated with low levels of *MIR156C* expression. The difference in the phenotype of plants doubly mutant for *val1-2* and mutations the PRC2 histone methyltransferases, *SWN* and *CLF*, and between *val1-2* and a mutation in the histone deacetylase *HDA19*, supports the hypothesis that the expression of *MIR156C* is regulated by a combination of histone marks. *val1-2; swn-3* and *val1-2; clf-29* double mutants have approximately the same amount of miR156 as *val1-2* single mutants, which is expected given that these genes are involved in the same process, namely the deposition of H3K27me3. In contrast, *hda19-3* significantly enhanced the level of miR156 compared to *val1-2*. This type of

606 genetic interaction is predicted if miR156 expression is dependent on histone
607 modifications aside from H3K27me3.

608 The evidence that *VAL1/VAL2* regulate the level, but not the temporal expression
609 pattern, of miR156 leaves open the question of how its temporal pattern arises. Several
610 other chromatin regulators, such as the CHD3 nucleosome remodeler PICKLE (Xu et
611 al., 2016b), the PRC-accessory protein LHP1 (Cui et al., 2020), the SWI/SNF2
612 chromatin remodeler BRAHMA (Xu et al., 2016c), and the histone 2 regulators ARP6
613 and HTA9/11 (Choi et al., 2016; Xu et al., 2018) have been found to play a role in the
614 expression of miR156. Furthermore, transcription factors including AGL15/18
615 (Serivichyaswat et al., 2015), MYB33 (Guo et al., 2017), and members of the *NF-Y*
616 family (Wei et al., 2017; Zhao et al., 2020), also regulate miR156 expression. It is
617 possible that the temporal expression pattern of miR156 is a consequence of complex
618 interactions between these diverse factors, rather than being dependent on a single
619 class of regulator, such as *VAL1/2*.
620
621 *VAL* genes and PRC1 activity

622 *VAL1/2* are thought to be necessary for the recruitment of PRC1 to target loci,
623 where it represses gene expression via PRC2-dependent and independent mechanisms
624 (Baile et al., 2020; Yuan et al., 2020; Zhou et al., 2017). We found that *VAL1/2*
625 accelerate vegetative phase change by repressing the expression of *MIR156A/C*, and
626 by indirectly promoting the expression of *SPL9*, a target of miR156. These results are
627 consistent with a previous study (Pico et al., 2015), which showed that *VAL1/2* and the
628 PRC1 components, AtBMI1A/B, repress *MIR156A/C* expression. However, the PRC1

components EMBRYONIC FLOWER1 (Pico et al., 2015) and RING1A/B (Li et al., 2017) have also been reported to repress the expression of *SPL9* independently of miR156. These latter effects delay vegetative phase change, which is the exact opposite of the effect produced by PRC1-mediated repression of *MIR156A/C*. Together, these results indicate that PRC1 can operate at different points within a regulatory pathway, or in interacting regulatory pathways, to modulate the output of the pathway or pathways. If the genes repressed by PRC1 have different functions—as in the case of miR156 and its *SPL* targets—then the functional significance of a particular level of PRC1 activity at a particular locus can be difficult to predict. These results also support the hypothesis that there may be different forms of PRC1, which target different genes. Moreover, our finding that H2AK119ub deposition at *SPL9* was unaffected in *val1-5(sd); val2-3* suggests that VAL1/2 may not be universally required for PRC1-recruitment.

In this regard, it is interesting that although *MIR156A* and *MIR156C* are close paralogs and have similar expression patterns, previous studies (Xu et al., 2018, 2016b), and the results presented here, indicate that these genes are differentially sensitive to mutations that affect the activity of PRC2 and PRC1. For example, we found that *val1; val2* mutants display a greater reduction in H2AK119ub and H3K27me3 at *MIR156C* than at *MIR156A*. Our findings align with the results of ChIP-seq studies of H2AK119ub and H3K27me3 in *atbmi1a/b/c* (Zhou et al., 2017) and *val1-2; val2-3* (Yuan et al., 2020) mutants. The implication of these observations is that *MIR156C* expression is more dependent on PRC1 and PRC2 activity than *MIR156A.* Defining the molecular basis for this difference could provide important insights into factors that influence epigenetic regulation in plants.

Unlike in animals, where PRC1 binding requires the prior deposition of H3K27me3, in plants PRC1 is thought to promote PRC2 activity at the majority of its targets (Calonje, 2014; Zhou et al., 2017). This model is supported by our results. In the case of *MIR156C*, we found that in 1 week old plants loss of *VAL1/2* significantly reduced H2AK119ub, but not H3K27me3. However, by 3 weeks both H2AK119ub and H3K27me3 were reduced in *val1/2* mutants. These results suggest that VAL1/2 and, by inference, PRC1 are present at *MIR156C* prior to PRC2, and promote the activity of PRC2.

In addition to their roles in vegetative phase change, *VAL* genes regulate multiple nodes of the flowering time (Jing et al., 2019; Qüesta et al., 2016; Yuan et al., 2016) and seed development (Chen et al., 2018, 2020; Suzuki et al., 2007; Yang et al., 2013a) networks. The co-option of *VAL* activity throughout genetic networks thus appears critical to coordinating plant developmental transitions. Despite the centrality of *VAL* function to the control of developmental timing, the persistent and robust pattern of *MIR156A/C* expression in *val* mutant plants emphasizes the complexity of temporal regulation in plants.

Materials and methods

Plant material and growth conditions

All stocks were grown in the Col-0 background. The following genetic lines have been described previously: *val1-2* (SALK_088606)*, val2-1* (CS906036) (Suzuki et al., 2007) (*val2-1* was backcrossed to Col-0 6 times from the original Wassilewskija parent); *val2-3* (SALK_059568C) (Yang et al., 2013a); *clf-29* (SALK_021003) (Bouveret et al., 2006);

675 *swn-3* (SALK_050195) (Chanvivattana et al., 2004); *hda19-3* (SALK_139445) (Kim et
676 al., 2008); *mir156a-2 mir156c-1 mir157a-1 mir157c-1* (He et al., 2018); *SPL9::rSPL9-*
677 *GUS* (Xu et al., 2016a); *val1-2 VAL1::VAL1-3xHA FRI-Sf2* (Qüesta et al., 2016). *val2-4*
678 (SALK_127961) was obtained from the Arabidopsis Biological Resources Center (Ohio
679 State University, OH, USA). Seeds were sown on fertilized Farfard #2 soil (Farfard) and
680 kept at 4°C for 3 days prior to transfer to a growth chamber, with the transfer day
681 counted as day 0 for plant age (0 DAG – days after germination). Plant were grown at
682 22°C under a mix of both white (USHIO F32T8/741) and red-enriched (Interlectric
683 F32/T8/WS Gro-Lite) fluorescent bulbs in either long day (16 hrs light/8 hrs. dark; 40
684 µmol m^{-2} s^{-1}) or short day (10 hrs light/14 hrs dark; 100 µmol m^{-2} s^{-1}) conditions.
685
686 **Identification of the *val1-5(sd)* mutant**
687 The *val1-5(sd)* allele was generated by exposing *mir157a-1; mir157c-1* seed to ethyl
688 methanesulfonate. An M2 mutant plant exhibiting delayed vegetative phase change was
689 backcrossed to the parental line and allowed to self. Tissue was pooled from 30 plants
690 exhibiting severely delayed vegetative phase change in the BC1F2 generation. DNA
691 was extracted via-SDS lysis and phenol-chloroform extraction and further purified using
692 Clean and Concentrator columns (Zymo Research). DNA concentration was determined
693 using a Qubit 2.0 Fluorometer (Invitrogen) and 1µg of DNA sheared using a Covaris S2
694 sonicator (Covaris) to produce 350bp inserts. Sequencing libraries were made following
695 the TruSeq DNA PCR-free LT Sample Prep Kit (Illumina) manufacturer's instructions.
696 Library quality and quantity was validated by Bioanalyser (Agilent) and KAPA analysis
697 (Kapa Biosystems). 100bp paired end reads were generated using a HiSeq 2500

(Illumina) and aligned to the TAIR10 reference genome following the default SHORE pipeline (Ossowski et al., 2008). The SHOREmap backcross pipeline (Schneeberger et al., 2009) using default options was employed to identify polymorphisms. Manual inspection of allele frequencies in the mutant revealed a peak centered on the *VAL1* locus. The causative mutation was confirmed by Sanger sequencing and complementation assays. The mutant was backcrossed to a 'Traffic Line' (Wu et al., 2015) with seed-fluorescent markers inserted adjacent to the *VAL1* locus to eliminate additional closely linked polymorphisms. Consequently, the resultant *val1-5(sd)* plants used in this study contain a linked *pNAP::RFP* insertion at 13,622,737bp on Chromosome 2 (Crick strand).

Generation of transgenic plants

For RY-mutation lines the RY-site TGCATG was replaced by TGTATG. A 5kb *MIR156C* genomic sequence including 2kb upstream of the transcriptional start site and 665bp downstream of the end of the last exon was cloned into the binary vector pAGM4723 from the Golden Gate MoClo toolbox supplied by Addgene (www.addgene.org) (Weber et al., 2011; Werner et al., 2012). For -RY3, -RY4 and -RY5 Q5 Site Directed Mutagenesis Kit (New England Biolabs) was used to induce a substitution directly into the expression vector. For -RY1, -RY2 and -RY12345 Gibson Assembly cloning (New England Biolabs) was used to assemble individual fragments into the same backbone. Golden Gate cloning was also used to generate *VAL1::VAL1-VAL1 3'UTR*, *VAL1::VAL1-GUS-VAL1 3'UTR*, *VAL1::GUS-VAL1 3'UTR* lines. Promoter/5'UTR (*VAL1*

- 2.3kb), functional (*VAL1* – 3.8kb, *MIR156A* (Fouracre and Poethig, 2019)) and 3'UTR/terminator (*VAL1* – 2kb) sequences were cloned separately from *Arabidopsis* gDNA, with Type II restriction sites removed where necessary. *GUS* and *AtuOCS* sequences were obtained from the MoClo Plant Parts toolkit supplied by Addgene (www.addgene.org) (Engler et al., 2014). Component parts were assembled using Golden Gate cloning into the pAGM4723 binary vector, including green or red seed fluorescent expression cassettes as selectable markers. Constructs were transformed into *Arabidopsis* using the floral dip method. All primers used for cloning are included in Supplementary table 1.

Quantification of gene expression

Tissue (either shoot apices with leaf primordia ≤1mm attached or isolated leaf primordia 0.5-1mm in size – as specified in the text) were ground in liquid nitrogen and total RNA extracted using Trizol (Invitrogen) as per the manufacturer's instructions. RNA was treated with RNAse-free DNAse (Qiagen) and 250ng-1µg of RNA was used for reverse transcription using Superscript III (Invitrogen). Gene specific RT primers were used to amplify miR156, miR157, miR172 and SnoR101 and a polyT primer for mRNA amplification. Three-step qPCR of cDNA was carried out using SYBR-Green Master Mix (Bimake). qPCR reactions were run in triplicate and an average was calculated. Relative transcript levels were normalized to snoR101 (for miRNAs) and *ACT2* (for mRNAs) and expressed as a ratio of expression to a specified control sample. The qPCR primers used in this study are listed in Supplementary table 1.

743 **Chromatin immunoprecipitation**

744 Expanded leaves and roots were removed during tissue harvesting to produce samples
745 enriched for shoot apices and young leaves. For histone ChIP ~0.5g of fresh tissue per
746 antibody and for anti-HA ChIP ~5g of fresh tissue were harvested. Samples were fixed
747 in 1% formaldehyde under vacuum for 15 minutes. Cross-linked samples were ground
748 in liquid nitrogen and suspended in Honda buffer (0.44M sucrose, 1.25% ficoll, 2.5%
749 dextran 40, 20mM hepes pH 7.4, 10mM $MgCl_2$, 0.5% Triton, 5mM DTT, 1mM PMSF,
750 1% protease inhibitors), filtered through two layers of Miracloth (EMD Millipore), and
751 pelleted and washed thrice in Honda buffer. For histone ChIP, pellets were
752 resuspended in nuclei lysis buffer (50mM Tris-HCl pH 8, 10mM EDTA, 1% SDS, 1%
753 protease inhibitors), for anti-HA ChIP, pellets were resuspended in RIPA buffer (1X
754 PBS, 1% NP-40, 0.5% sodium deoxycholate, 0.1% SDS, 1% protease inhibitors).
755 Samples were sonicated using a Fisherbrand Sonic Dismembrator (Fisher Scientific) 6x
756 10s at setting 3.2. ChIP samples were pre-cleared using Dynabeads Protein A
757 (Invitrogen). 2% was removed as input and samples were incubated overnight with 1%
758 antibody (for histone ChIP: anti-H3 (abcam ab1791), anti-H3K27me3 (EMD Millipore 07-
759 449), anti-H2AK119ub (Cell Signaling Technology 8240); for VAL1-HA ChIP: anti-HA
760 (Roche 11583816001)). Chromatin-antibody conjugates were purified with Dynabeads
761 Protein A and washed in low/high salt, lithium and TE buffers. Following reverse-
762 crosslinking DNA was isolated using a QIAquick PCR Purification Kit (Qiagen).

763 For ChIP-qPCR assays, three-step qPCR was carried out using SYBR-Green
764 Master Mix (Bimake). qPCR reactions were run in triplicate and an average was
765 calculated. Data were normalized and presented as follows: 1) For H3K27me3 – *STM*

766 was used as a control locus, data is presented as a ratio of (H3K27me3 gene of
767 interest/H3 gene of interest) to (H3K27me3 *STM*/H3 *STM*); 2) For H2AK119ub – *ACT7*
768 was used as a control locus, data is presented as a ratio of (H2AK119ub gene of
769 interest/input gene of interest) to (H2AK119ub *ACT7*/input *ACT7*); 3) For VAL1-HA –
770 *UBQ10, ACT7* and *TA3* were used as control loci, data is presented as a ratio of
771 ((VAL1-HA ChIP gene of interest/input gene of interest)/(VAL1-HA ChIP control/input
772 control)) relative to ((WT ChIP gene of interest/input gene of interest)/(WT ChIP
773 control/input control)). The qPCR primers used in this study are listed in Supplementary
774 table 1.
775
776 **Mass spectrometry**
777 *VAL1::VAL1-3xHA; val1-2; FRI-Sf2* and *val1-2* genotypes were used as experimental
778 and control samples respectively. Expanded leaves and roots were removed during
779 tissue harvesting to produce samples enriched for shoot apices and young leaves. 2-3g
780 of fresh tissue was harvested for immunoprecipitation, 0.2-0.6g was harvested for total
781 protein extraction. For immunoprecipitation, tissue was ground in liquid nitrogen,
782 suspended in IP buffer (20mM Tris-HCl pH 8, 150mM NaCl, 2.5mM EDTA, 0.5% Triton,
783 1% protease inhibitors, 1mM PMSF), rotated for 2 hours at 4^{o}C and filtered through 2
784 layers of Miracloth. Anti-HA (Roche) conjugated Dynabeads Protein A (Invitrogen) were
785 added and samples were rotated overnight at 4^{o}C. Beads were washed thrice with IP
786 buffer and proteins were purified for mass spectrometry using an S-Trap: Rapid
787 Universal MS Sample Prep (Protifi) following the manufacturer's instructions. For total
788 proteomes, ground tissue was suspended in 8M urea and rotated at room temperature

for 45 minutes. The samples were centrifuged thrice and the supernatant reduced with DTT (final concentration 5mM) and alkylated with iodoacetamide 40 (final concentration 40mM) before overnight digest with trypsin. Samples were resuspended in 10 µl of water + 0.1% TFA and loaded onto a Dionex RSLC Ultimate 300 (Thermo Scientific, San Jose, CA, USA), coupled online with an Orbitrap Fusion Lumos (Thermo Scientific). Chromatographic separation was performed with a two-column system, consisting of a C_{18} trap cartridge (300 µm ID, 5 mm length) and a picofrit analytical column (75 µm ID, 25 cm length) packed in-house with reversed-phase Repro-Sil Pur C_{18}-AQ 3 µm resin. Peptides were separated using a 90 min gradient (for the IP experiments) and 180 min (for the full proteome experiment) from 2-28% buffer-B (buffer-A: 0.1% formic acid, buffer-B: 80% acetonitrile + 0.1% formic acid) at a flow rate of 300 nl/min. The mass spectrometer was set to acquire spectra in a data-dependent acquisition (DDA) mode. Briefly, the full MS scan was set to 300-1200 m/z in the orbitrap with a resolution of 120,000 (at 200 m/z) and an AGC target of 5x10e5. MS/MS was performed in the ion trap using the top speed mode (2 secs), an AGC target of 10e4 and an HCD collision energy of 30. Raw files were searched using Proteome Discoverer software (v2.4, Thermo Scientific) using SEQUEST as search engine using the SwissProt *Arabidopsis thaliana* database. The search for total proteome included variable modifications of methionine oxidation and N-terminal acetylation, and fixed modification of carbamidomethyl cysteine. Trypsin was specified as the digestive enzyme. Mass tolerance was set to 10 pm for precursor ions and 0.2 Da for product ions. Peptide and protein false discovery rate was set to 1%. Data transformation, normalization and

811 statistical analysis using heteroscedastic t-test was performed as previously described
812 (Aguilan et al., 2020).
813 Proteins were sorted according to their descending or ascending linearity across
814 the three weeks. To do so, we used a custom score taking into account monotonic
815 trend, reproducibility across replicates and magnitude of change across weeks. The 50
816 proteins with the highest descending and ascending trend scores were used to identify
817 enriched GO terms for biological processes using the Fisher's Exact PANTHER
818 Overrepresentation Test (released 2020-07-28) and GO Ontology database DOI:
819 10.5281/zenodo.4081749 (released 2020-10-09). The *Arabidopsis thaliana* genome
820 was used as a reference list. Protein interaction maps for the same sets of 50 proteins
821 were made using the STRING app from Cytoscape (Shannon et al., 2003).
822
823 **GUS staining and histology**
824 Shoot apices and whole plants were fixed in 90% acetone on ice for 10 minutes,
825 washed with GUS staining buffer (5mM potassium ferricyanide and 5mM ferrocyanide in
826 0.1M PO_4 buffer) and incubated at 37°C overnight in GUS staining buffer with 2mM X-
827 Gluc. Embryos were placed directly in X-Gluc (GoldBio) GUS staining buffer and
828 incubated for 1hr. To quantify GUS activity, a 4-methylumbelliferyl b-D-glucuronide
829 (MUG) (Sigma-Aldrich) assay was carried out as previously described (He et al., 2018).
830 For histological observations individuals were fixed in FAA (3.7% formaldehyde),
831 dehydrated in an ethanol series and cleared using Histo-Clear (National Diagnostics).
832 Following embedding in Paraplast Plus (Sigma-Aldrich) 8μM sections were produced

using an HM 355 microtome (Microm) and visualized using an Olympus BX51 microscope with a DP71 camera attachment (Olympus).

Quantification and statistical analyses

Details of all statistical analyses, including the type of statistical test, sample size, replicate number and significance threshold, are included in the relevant figure legend. For figures featuring boxplots, boxes display the IQR (boxes), median (lines), and values beyond 1.5* IQR (whiskers); mean values are marked by a solid diamond (◆). Statistical analyses were carried out using RStudio (RStudio Team, 2020) and Microsoft Excel. Measurements of leaf shape were made using ImageJ (Schindelin et al., 2012).

Materials Availability

The *val1-5(sd), val1-5(sd); val2-3*, *val1-2; val2-4, val1-2; mir156ac mir157ac* and *VAL1::VAL1-GUS-VAL1 3'UTR* lines described herein have been donated to the ABRC (stock numbers CS72451-CS72455 respectively). All other plant lines and plasmids generated during this project are available on request to Scott Poethig (spoethig@sas.upenn.edu).

Acknowledgements

We thank members of the R.S.P laboratory and Doris Wagner (University of Pennsylvania) for helpful discussions, Daniel Martinez and Ryan McCarthy (University of Pennsylvania) for assistance with histology and chromatin sonication, the Arabidopsis Biological Resource Center for T-DNA insertion lines and Julia Qüesta and Caroline

Dean (John Innes Center) for the kind donation of *VAL1-HA; val1-2; FRI-Sf2* seed. This project was funded by NIH Grant GM051893 (to R.S.P). S.S. gratefully acknowledges Merck/MSD for the Umberto Mortari Award (2019), the Japan Agency for Medical Research and Development (AMED) and the New York Academy of Sciences (NYAS) for supporting aging research in his lab.

Author Contributions

Conceptualization: J.P.F., R.S.P.; Methodology: J.P.F., R.S.P.; Investigation: J.P.F., J.H., V.J.C., S.S.; Formal analysis: J.P.F., S.S.; Resources: J.P.F., J.H.; Visualization: J.P.F., S.S.; Writing - original draft: J.P.F.; Writing - review & editing: J.P.F., J.H., S.S., R.S.P.; Supervision: R.S.P.; Project administration: R.S.P.; Funding acquisition: R.S.P.

Declaration of Interests

The authors declare no competing interests.

Supplemental files titles and legends

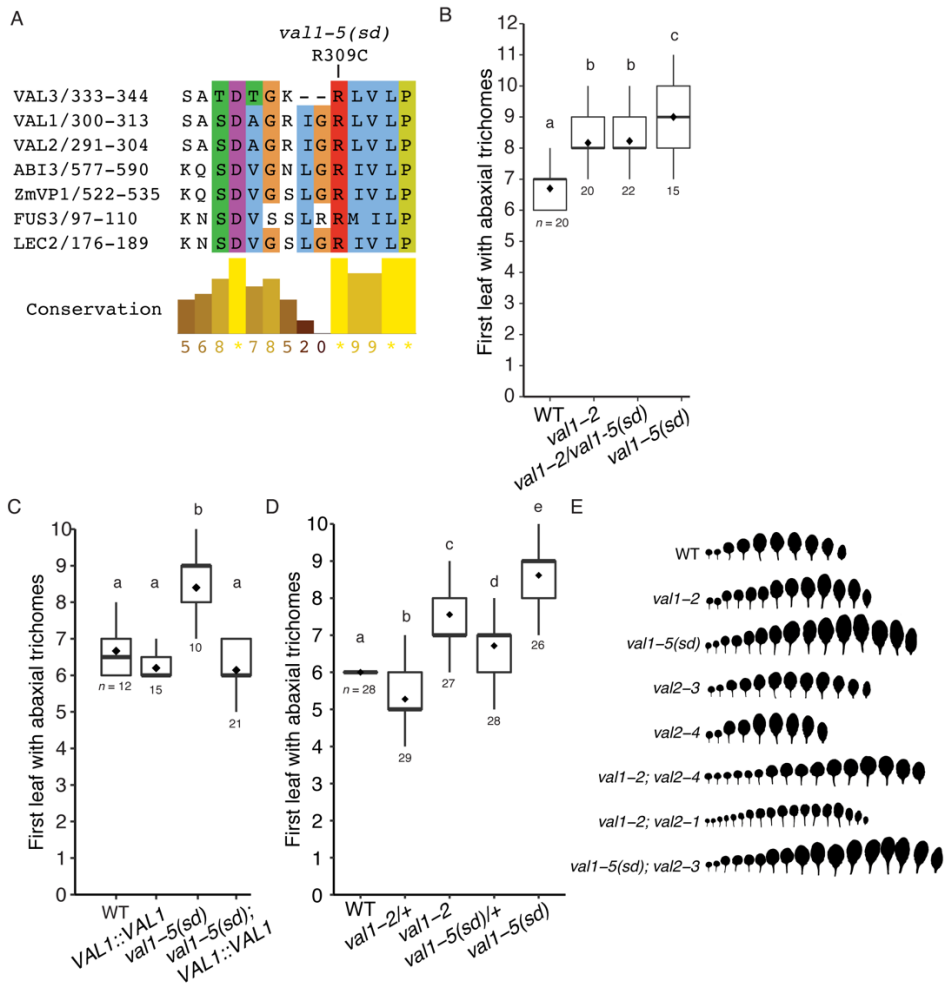

Supplementary file 1. *val1-5(sd)* is an antimorphic allele

(A) Sequence alignment of the B3 DNA-binding domain N-arm of *Arabidopsis* LAV family members and the maize ABI3 ortholog VP1. Numbers correspond to amino acid sequence numbers, colors correspond to the ClustalX amino acid color scheme. In the *val1-5(sd)* mutant a C>T base substitution converts an arginine to a cysteine.

(B) *val1-5(sd)* complementation test with the null *val1-2* allele

(C) Rescue of the *val1-5(sd)* abaxial trichome phenotype with a *VAL1* genomic sequence. Independent T1 lines are shown.

884 (D) Allele heterozygosity testing. (B-D) Boxes display the interquartile range (IQR)
885 (boxes), median (lines) and values beyond 1.5*IQR (whiskers); mean values are
886 marked by ◆. Samples sizes are displayed on the graph. Statistically distinct
887 genotypes were identified by one-way ANOVA with *post hoc* Tukey multiple
888 comparison test (letters indicate statistically distinct groups; $P < 0.05$), all plants
889 grown in LD.
890 (E) Heteroblastic series of lines shown in Figure 1.
891

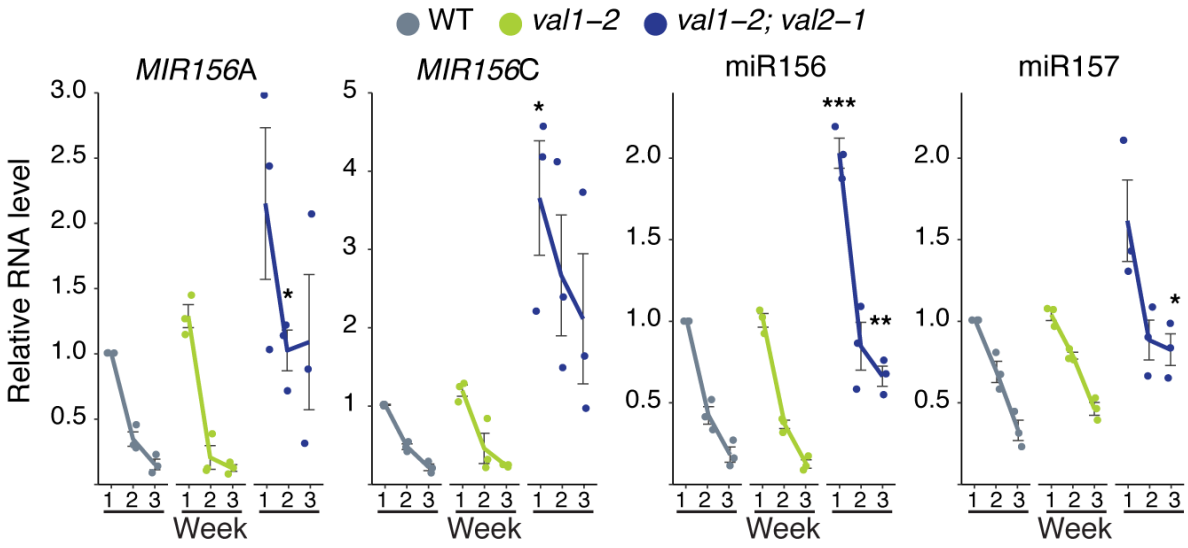

Supplementary file 2. *VAL* genes redundantly regulate miR156 expression

qRT-PCR analyses of gene expression in shoot apices with leaf primordia (LP) ≥ 1mm removed at 1, 2 and 3 weeks. All plants were grown in SD conditions. Each data point represents a biological replicate and is the average of three technical replicates. Coloured lines represent the mean and black lines mean±s.e.m. Asterisks represent significant differences between WT and *val* mutants at the same time point, calculated by an unpaired two-tailed *t*-test with a Bonferroni correction for multiple comparisons (* $P < 0.025$; ** $P < 0.005$; *** $P < 0.0005$).

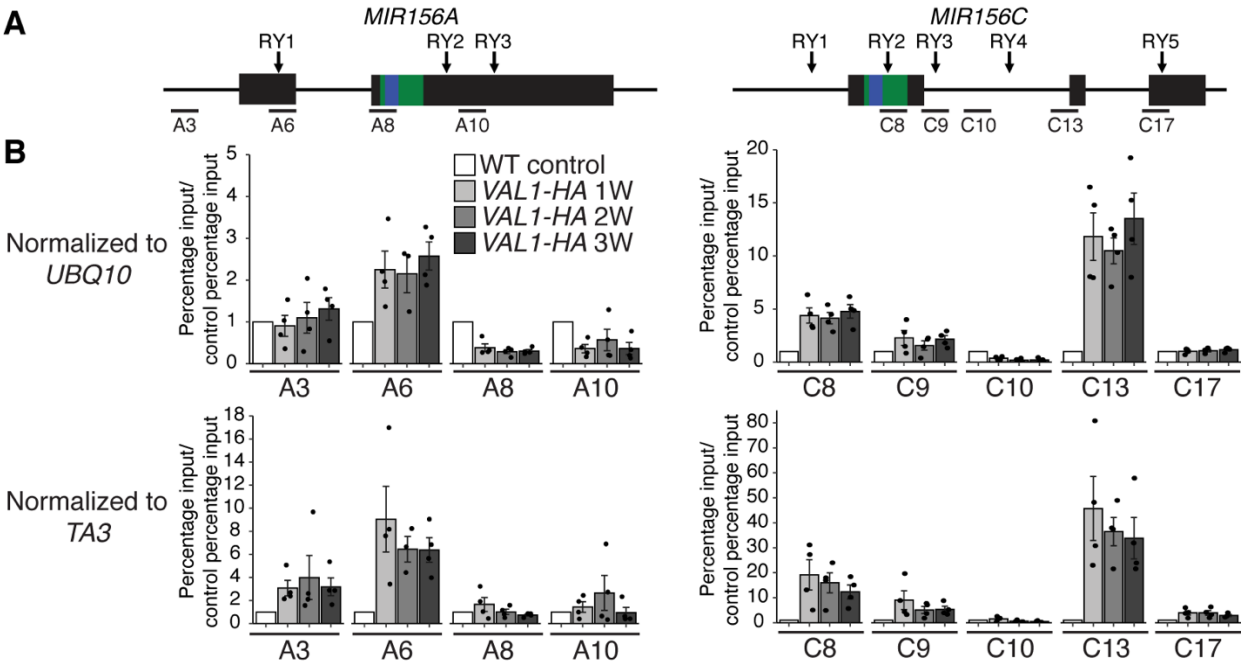

902

903 **Supplementary file 3. VAL1 binds consistently to *MIR156A* and *MIR156C* during**

904 **vegetative development**

905 (A) Schematic depicting the location of primers used for ChIP-qPCR, the sequences

906 encoding the miR156 hairpin and mature miRNA are coloured green and blue

907 respectively.

908 (B) Anti-HA ChIP-qPCR of WT Col control plants at 2W and *VAL1::VAL1-HA; val1-2;*

909 *FRI-Sf2* plants at 1, 2 and 3W of growth. The data is presented as percentage

910 input normalized to a control locus (*UBQ10* or *TA3*) and is displayed relative to

911 WT. Each data point represents a biological replicate and is the average of three

912 technical replicates, bars represent the mean and error bars the mean±s.e.m.

913 Plants were grown in SD conditions.

914

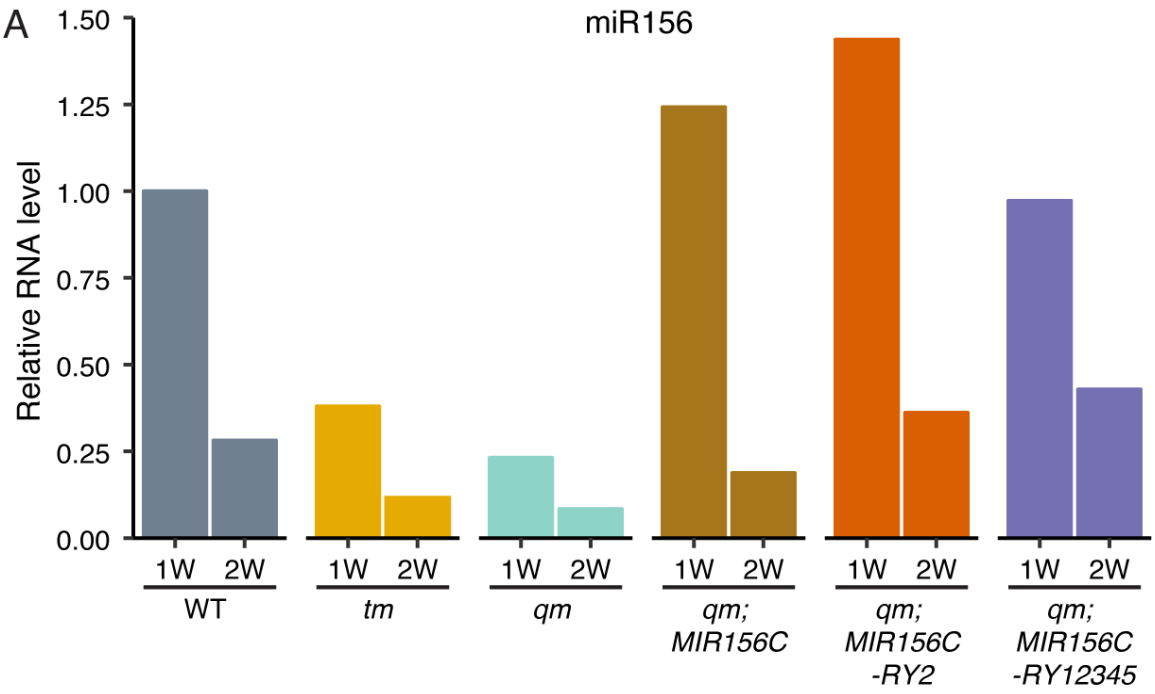

Supplementary file 4. RY sites are not required for the temporal decline of *MIR156C*

(A) qRT-PCR analyses of gene expression in shoot apices with LP ≥ 1mm removed at 1 and 2 weeks. Bars represent the average of three technical replicates for a single biological replicate of pooled T1 plants, at least 15 independent T1 plants were pooled for each sample. *qm = mir156a mir156c mir157a mir157c quadruple mutant, tm = mir156a mir157a mir157c triple mutant*. Plants were grown in SD conditions.

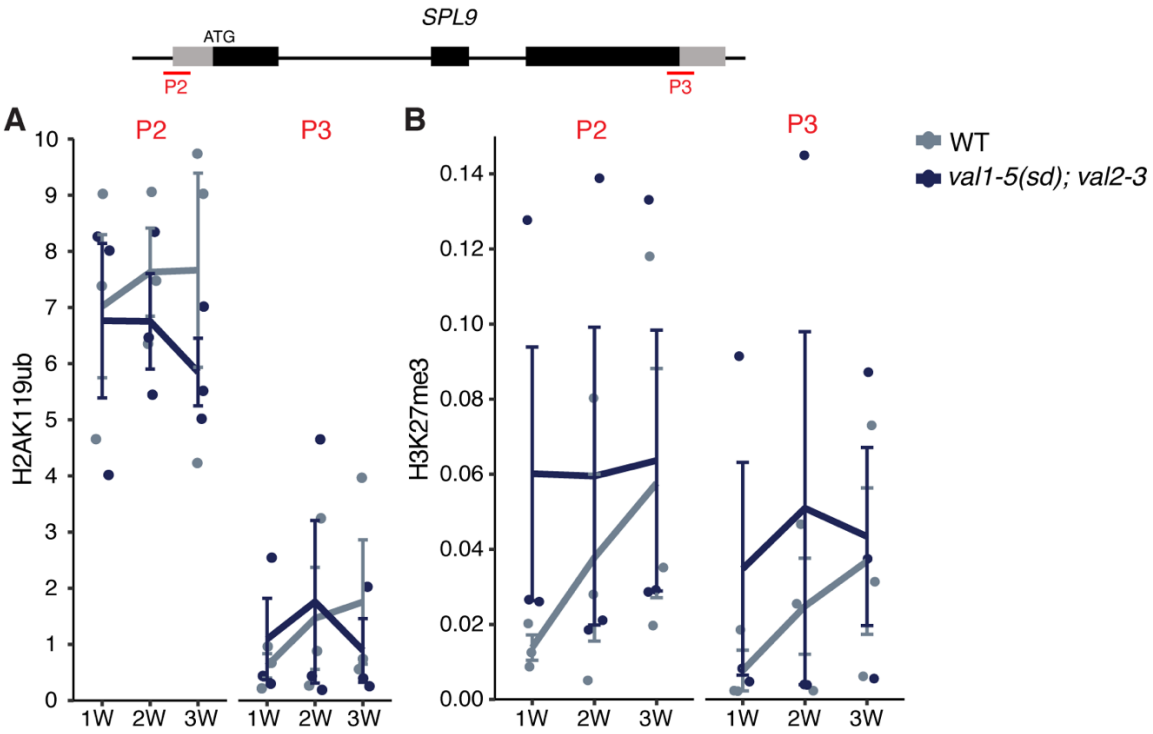

Supplementary file 5. *VAL* genes do not regulate *SPL9* chromatin state

(A, B) Temporal analysis of histone modification scalculated by ChIP-qPCR. Each data point represents a biological replicate and is the average of three technical replicates. Lines represent the mean and bars represent the mean±s.e.m., (A) H3K2me3 values are relative to H3 and normalised to *STM* as an internal control. (B) H2AK119ub values are relative to input and normalised to *ACT7* as an internal control. Plants were grown in SD conditions.

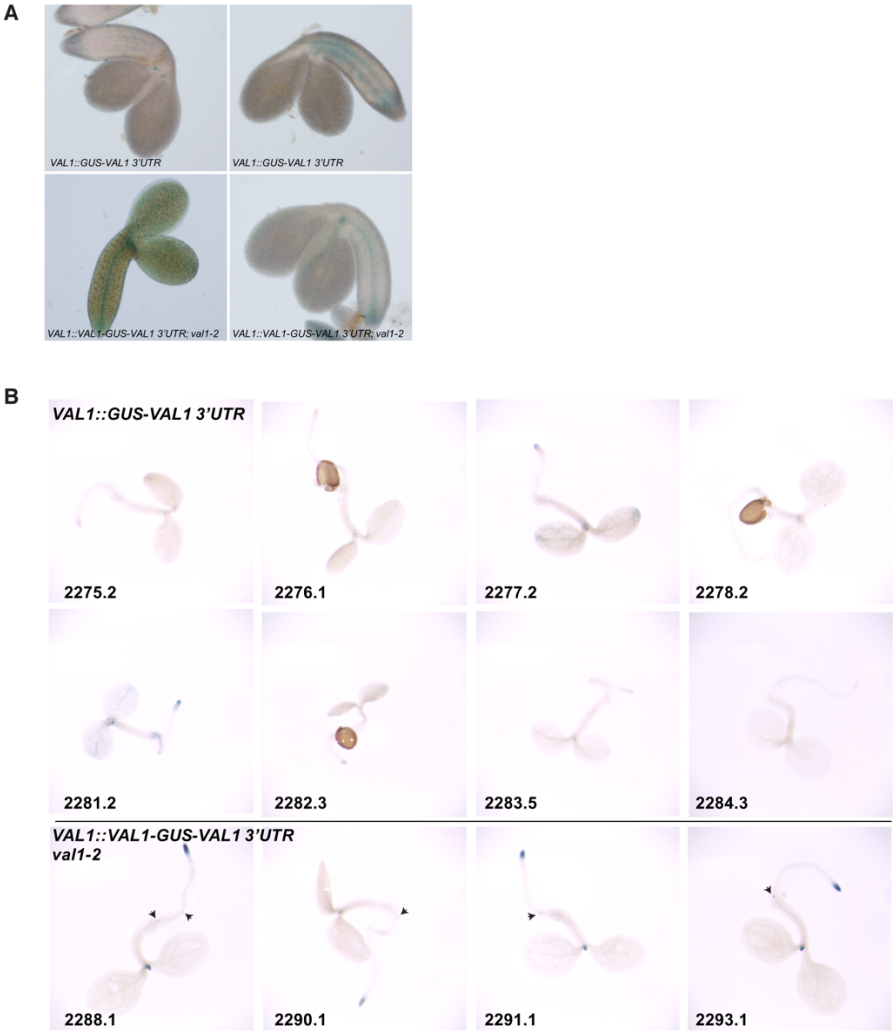

934

935 **Supplementary file 6. *VAL1* expression is dependent on genetic elements in the**

936 **coding sequence of the gene**

937 (A) Torpedo-stage embryos of two-independent homozygous transgenic lines each

938 expressing a transcriptional (top panel) or translational (bottom panel) *VAL1-*

939 *GUS* reporter construct.

940 (B) Seedlings at 3 DAG. Each number designates an independent homozygous

941 transgenic line. Arrow heads point to initiating lateral root primordia. All plants

942 were grown in LD.

943

A

Ascending Cluster			Descending Cluster		
GO Term	*P* value	FDR	GO Term	*P* value	FDR
response to cadmium ion (GO:0046686)	1.71E-14	5.12E-11	response to cold (GO:0009409)	2.81E-20	1.68E-16
response to cold (GO:0009409)	4.12E-09	3.08E-06	response to cadmium ion (GO:0046686)	4.90E-13	5.86E-10
response to water deprivation (GO:0009414)	4.18E-06	1.14E-03	reductive pentose-phosphate cycle (GO:0019253)	1.84E-10	7.34E-08
nucleocytoplasmic transport (GO:0006913)	5.19E-05	1.00E-02	defense response to bacterium (GO:0042742)	4.03E-09	1.10E-06
response to zinc ion (GO:0010043)	7.59E-05	1.26E-02	gluconeogenesis (GO:0006094)	1.64E-07	2.89E-05
ribosomal large subunit assembly (GO:0000027)	8.11E-05	1.31E-02	fructose 1,6-bisphosphate metabolic process (GO:0030388)	2.53E-06	3.29E-04
toxin catabolic process (GO:0009407)	9.81E-05	1.50E-02	response to sucrose (GO:0009744)	1.01E-05	1.02E-03
defense response to bacterium (GO:0042742)	1.10E-04	1.60E-02	pentose-phosphate shunt (GO:0006098)	3.87E-05	3.35E-03
positive regulation of protein-containing complex disassembly (GO:0043243)	1.16E-04	1.65E-02	response to light stimulus (GO:0009416)	4.30E-05	3.57E-03
unidimensional cell growth (GO:0009826)	1.87E-04	2.54E-02	ATP synthesis coupled proton transport (GO:0015986)	7.59E-05	5.90E-03
cellular response to hydrogen peroxide (GO:0070301)	2.49E-04	3.11E-02	ammonia assimilation cycle (GO:0019676)	9.00E-05	6.41E-03
response to abscisic acid (GO:0009737)	2.94E-04	3.59E-02	photosynthetic electron transport chain (GO:0009767)	9.22E-05	6.49E-03
translation (GO:0006412)	3.34E-04	3.70E-02	glycine decarboxylation via glycine cleavage system (GO:0019464)	1.16E-04	7.85E-03
			defense response to fungus, incompatible interaction (GO:0009817)	1.24E-04	8.07E-03
			carbon utilization (GO:0015976)	1.44E-04	9.28E-03
			glycolytic process (GO:0006096)	1.54E-04	9.51E-03
			protein folding (GO:0006457)	3.58E-04	1.96E-02
			plastid translation (GO:0032544)	7.31E-04	3.80E-02
			chloroplast organization (GO:0009658)	9.79E-04	4.96E-02

B

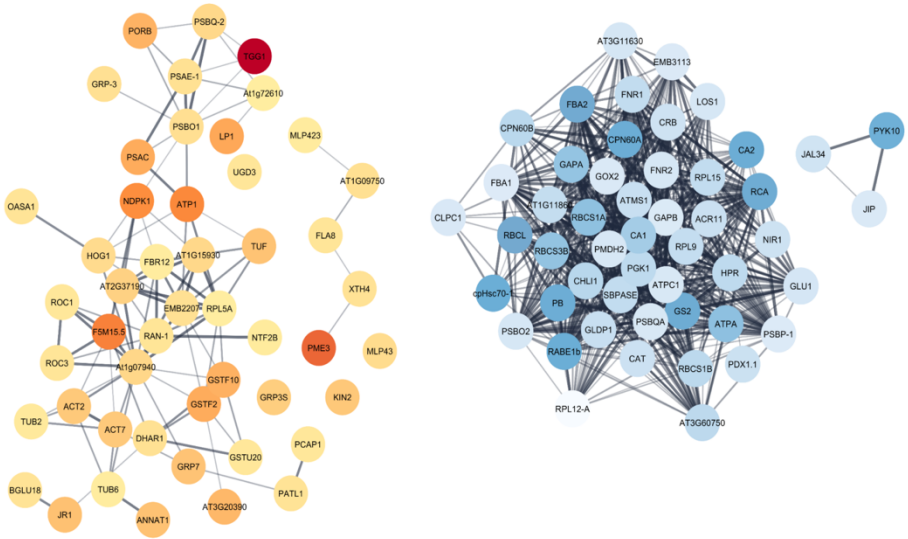

Supplementary file 7. Proteomic changes during vegetative development

(A,B) The 50 proteins with the strongest increasing or decreasing trend score during vegetative development in the experimental sample only (see Methods for details). (A) GO terms enriched within the 50 proteins that have the strongest increasing or decreasing trend score. (G) Interaction networks for each set of 50 proteins, the darker the color the stronger the increasing (red) or decreasing (blue) trend score.

953 **Supplementary table 1. Primer sequences**

954 This table includes all the primer sequences used in this study.

955

956 **Supplementary table 2. Proteins detected by mass spectrometry following anti-**

957 **HA immunoprecipitation**

958 Related to Supplementary file 6.

959 This table includes the raw mass spectrometry results and data processing for IP-

960 samples.

961

962 **Supplementary table 3. Total proteome changes during vegetative development**

963 Related to Supplementary file 6.

964 This table includes the raw mass spectrometry results and data processing for total

965 proteome samples.

966

967 **References**

968 Aguilan, J.T., Kulej, K., and Sidoli, S. (2020). Guide for protein fold change and p-value
969 calculation for non-experts in proteomics. Mol. Omics *16*, 573–582.

970 Baile, F., Merini, W., Hidalgo, I., and Calonje, M. (2020). Dissection of PRC1 and PRC2
971 recruitment in Arabidopsis connects EAR repressome to PRC2 anchoring. BioRxiv
972 2020.08.28.271999.

973 Beydler, B., Osadchuk, K., Cheng, C.-L., Manak, J.R., and Irish, E.E. (2016). The Juvenile Phase of
974 Maize Sees Upregulation of Stress-Response Genes and Is Extended by Exogenous Jasmonic
975 Acid. Plant Physiol. *171*, 2648–2658.

976 Bouveret, R., Schönrock, N., Gruissem, W., and Hennig, L. (2006). Regulation of flowering time
977 by *Arabidopsis MSI1*. Development *133*, 1693–1702.

978 Bratzel, F., López-Torrejón, G., Koch, M., Del Pozo, J.C., and Calonje, M. (2010). Keeping Cell
979 Identity in Arabidopsis Requires PRC1 RING-Finger Homologs that Catalyze H2A
980 Monoubiquitination. Current Biology *20*, 1853–1859.

981 Calonje, M. (2014). PRC1 Marks the Difference in Plant PcG Repression. Molecular Plant *7*, 459–
982 471.

983 Carbonero, P., Iglesias-Fernández, R., and Vicente-Carbajosa, J. (2017). The AFL subfamily of B3
984 transcription factors: evolution and function in angiosperm seeds. Journal of Experimental
985 Botany *68*, 871–880.

986 Chanvivattana, Y., Bishopp, A., Schubert, D., Stock, C., Moon, Y.-H., Sung, Z.R., and Goodrich, J.
987 (2004). Interaction of Polycomb-group proteins controlling flowering in *Arabidopsis*.
988 Development *131*, 5263–5276.

989 Chen, N., Veerappan, V., Abdelmageed, H., Kang, M., and Allen, R.D. (2018). HSI2/VAL1 Silences
990 *AGL15* to Regulate the Developmental Transition from Seed Maturation to Vegetative Growth
991 in Arabidopsis. Plant Cell *30*, 600–619.

992 Chen, N., Wang, H., Abdelmageed, H., Veerappan, V., Tadege, M., and Allen, R.D. (2020).
993 HSI2/VAL1 and HSL1/VAL2 function redundantly to repress DOG1 expression in Arabidopsis
994 seeds and seedlings. New Phytologist *227*, 840–856.

995 Chhun, T., Chong, S.Y., Park, B.S., Wong, E.C.C., Yin, J.-L., Kim, M., and Chua, N.-H. (2016). HSI2
996 Repressor Recruits MED13 and HDA6 to Down-Regulate Seed Maturation Gene Expression
997 Directly During Arabidopsis Early Seedling Growth. Plant and Cell Physiology *57*, 1689–1706.

998 Choi, K., Kim, J., Muller, S.Y., Oh, M., Underwood, C., Henderson, I., and Lee, I. (2016).
999 Regulation of microRNA-mediated developmental changes by the SWR1 chromatin remodeling
1000 complex. Plant Physiol *171*, 1128–1143.

1001 Cui, Y., Cheng, J., Ruan, S., Qi, P., Liu, W., Bian, H., Ye, L., Zhang, Y., Hu, J., Dong, G., et al. (2020).
1002 The heterochronic gene Oryza sativa LIKE HETEROCHROMATIN PROTEIN 1 modulates
1003 miR156b/c/i/e levels. Journal of Integrative Plant Biology *62*, 1839–1852.

1004 Engler, C., Youles, M., Gruetzner, R., Ehnert, T.M., Werner, S., Jones, J.D., Patron, N.J., and
1005 Marillonnet, S. (2014). A golden gate modular cloning toolbox for plants. ACS Synth. Biol. *3*,
1006 839–843.

1007 Fouracre, J.P., and Poethig, R.S. (2019). Role for the shoot apical meristem in the specification
1008 of juvenile leaf identity in *Arabidopsis*. Proc Natl Acad Sci USA *116*, 10168–10177.

1009 German, M.A., Pillay, M., Jeong, D.-H., Hetawal, A., Luo, S., Janardhanan, P., Kannan, V.,
1010 Rymarquis, L.A., Nobuta, K., German, R., et al. (2008). Global identification of microRNA–target
1011 RNA pairs by parallel analysis of RNA ends. Nature Biotechnology *26*, 941–946.

Goodrich, J., Puangsomlee, P., Martin, M., Long, D., Meyerowitz, E.M., and Coupland, G. (1997). A Polycomb-group gene regulates homeotic gene expression in Arabidopsis. Nature *386*, 44–51.

Gou, J.Y., Felippes, F.F., Liu, C.J., Weigel, D., and Wang, J.W. (2011). Negative regulation of anthocyanin biosynthesis in Arabidopsis by a miR156-targeted SPL transcription factor. Plant Cell *23*, 1512–1522.

Guo, C., Xu, Y., Shi, M., Lai, Y., Wu, X., Wang, H., Zhu, Z., Poethig, R.S., and Wu, G. (2017). Repression of miR156 by miR159 regulates the timing of the juvenile-to-adult transition in *Arabidopsis*. Plant Cell *29*, 1293–1304.

Guo, X., Hou, X., Fang, J., Wei, P., Xu, B., Chen, M., Feng, Y., and Chu, C. (2013). The rice *GERMINATION DEFECTIVE 1*, encoding a B3 domain transcriptional repressor, regulates seed germination and seedling development by integrating GA and carbohydrate metabolism. The Plant Journal *75*, 403–416.

He, J., Xu, M., Willmann, M.R., McCormick, K., Hu, T., Yang, L., Starker, C.G., Voytas, D.F., Meyers, B.C., and Poethig, R.S. (2018). Threshold-dependent repression of *SPL* gene expression by miR156/miR157 controls vegetative phase change in *Arabidopsis thaliana*. PLoS Genet. *14*, e1007337.

Huijser, P., and Schmid, M. (2011). The control of developmental phase transitions in plants. Development *138*, 4117–4129.

Jang, I.-C., Chung, P.J., Hemmes, H., Jung, C., and Chua, N.-H. (2011). Rapid and Reversible Light-Mediated Chromatin Modifications of Arabidopsis *Phytochrome A* Locus. Plant Cell *23*, 459–470.

Jing, Y., Guo, Q., and Lin, R. (2019). The B3-Domain Transcription Factor VAL1 Regulates the Floral Transition by Repressing *FLOWERING LOCUS T*. Plant Physiol. *181*, 236–248.

Kagaya, Y., Ohmiya, K., and Hattori, T. (1999). RAV1, a novel DNA-binding protein, binds to bipartite recognition sequence through two distinct DNA-binding domains uniquely found in higher plants. Nucleic Acids Research *27*, 470–478.

Kim, K.-C., Lai, Z., Fan, B., and Chen, Z. (2008). *Arabidopsis* WRKY38 and WRKY62 Transcription Factors Interact with Histone Deacetylase 19 in Basal Defense. Plant Cell *20*, 2357–2371.

Lawrence, E.H., Springer, C.J., Helliker, B.R., and Poethig, R.S. (2020). MicroRNA156-mediated changes in leaf composition lead to altered photosynthetic traits during vegetative phase change. New Phytologist.

Leichty, A.R., and Poethig, R.S. (2019). Development and evolution of age-dependent defenses in ant-acacias. Proc Natl Acad Sci USA *116*, 15596–15601.

Li, J., Wang, Z., Hu, Y., Cao, Y., and Ma, L. (2017). Polycomb Group Proteins RING1A and RING1B Regulate the Vegetative Phase Transition in Arabidopsis. Frontiers in Plant Science *8*, 867.

Lopez-Vernaza, M., Yang, S., Müller, R., Thorpe, F., de Leau, E., and Goodrich, J. (2012). Antagonistic Roles of SEPALLATA3, FT and FLC Genes as Targets of the Polycomb Group Gene CURLY LEAF. PLOS ONE *7*, e30715.

Mao, Y.-B., Liu, Y.-Q., Chen, D.-Y., Chen, F.-Y., Fang, X., Hong, G.-J., Wang, L.-J., Wang, J.-W., and Chen, X.-Y. (2017). Jasmonate response decay and defense metabolite accumulation contributes to age-regulated dynamics of plant insect resistance. Nature Communications *8*, 13925.

Molitor, A.M., Bu, Z., Yu, Y., and Shen, W.-H. (2014). Arabidopsis AL PHD-PRC1 Complexes Promote Seed Germination through H3K4me3-to-H3K27me3 Chromatin State Switch in Repression of Seed Developmental Genes. PLOS Genetics *10*, e1004091.

Ossowski, S., Schneeberger, K., Clark, R.M., Lanz, C., Warthmann, N., and Weigel, D. (2008). Sequencing of natural strains of Arabidopsis thaliana with short reads. Genome Res *18*, 2024–2033.

Pico, S., Ortiz-Marchena, M.I., Merini, W., and Calonje, M. (2015). Deciphering the role of Polycomb Repressive Complex 1 (PRC1) variants in regulating the acquisition of flowering competence in Arabidopsis. Plant Physiology *168*, 1286–1297.

Qüesta, J.I., Song, J., Geraldo, N., An, H., and Dean, C. (2016). *Arabidopsis* transcriptional repressor VAL1 triggers Polycomb silencing at *FLC* during vernalization. Science *353*, 485–488.

Ronemus, M., Vaughn, M.W., and Martienssen, R.A. (2006). MicroRNA-Targeted and Small Interfering RNA–Mediated mRNA Degradation Is Regulated by Argonaute, Dicer, and RNA-Dependent RNA Polymerase in *Arabidopsis*. Plant Cell *18*, 1559–1574.

RStudio Team (2020). RStudio: Integrated Development Environment for R (Boston, MA: RStudio, PBC).

Sasnauskas, G., Kauneckaitė, K., and Siksnys, V. (2018). Structural basis of DNA target recognition by the B3 domain of Arabidopsis epigenome reader VAL1. Nucleic Acids Research *46*, 4316–4324.

Schindelin, J., Arganda-Carreras, I., Frise, E., Kaynig, V., Longair, M., Pietzsch, T., Preibisch, S., Rueden, C., Saalfeld, S., Schmid, B., et al. (2012). Fiji: an open-source platform for biological-image analysis. Nature Methods *9*, 676–682.

Schneeberger, K., Ossowski, S., Lanz, C., Juul, T., Petersen, A.H., Nielsen, K.L., Jorgensen, J.E., Weigel, D., and Andersen, S.U. (2009). SHOREmap: simultaneous mapping and mutation identification by deep sequencing. Nat Methods *6*, 550–551.

1079 Serivichyaswat, P., Ryu, H.S., Kim, W., Kim, S., Chung, K.S., Kim, J.J., and Ahn, J.H. (2015).
1080 Expression of the floral repressor miRNA156 is positively regulated by the AGAMOUS-like
1081 proteins AGL15 and AGL18. Mol Cells *38*, 259–266.

1082 Shannon, P., Markiel, A., Ozier, O., Baliga, N.S., Wang, J.T., Ramage, D., Amin, N., Schwikowski,
1083 B., and Ideker, T. (2003). Cytoscape: A Software Environment for Integrated Models of
1084 Biomolecular Interaction Networks. Genome Research *13*, 2498–2504.

1085 Suzuki, M., Kao, C.Y., and McCarty, D.R. (1997). The conserved B3 domain of VIVIPAROUS1 has a
1086 cooperative DNA binding activity. Plant Cell *9*, 799–807.

1087 Suzuki, M., Wang, H.H.-Y., and McCarty, D.R. (2007). Repression of the *LEAFY COTYLEDON 1/B3*
1088 Regulatory Network in Plant Embryo Development by *VP1/ABSCISIC ACID INSENSITIVE 3-LIKE* B3
1089 Genes. Plant Physiol. *143*, 902–911.

1090 Telfer, A., Bollman, K.M., and Poethig, R.S. (1997). Phase change and the regulation of trichome
1091 distribution in *Arabidopsis thaliana*. Development *124*, 645–654.

1092 Tian, R., Wang, F., Zheng, Q., Niza, V.M.A.G.E., Downie, A.B., and Perry, S.E. (2020). Direct and
1093 indirect targets of the arabidopsis seed transcription factor ABSCISIC ACID INSENSITIVE3. The
1094 Plant Journal *103*, 1679–1694.

1095 Tsukagoshi, H., Morikami, A., and Nakamura, K. (2007). Two B3 domain transcriptional
1096 repressors prevent sugar-inducible expression of seed maturation genes in *Arabidopsis*
1097 seedlings. Proc Natl Acad Sci USA *104*, 2543–2547.

1098 Veerappan, V., Wang, J., Kang, M., Lee, J., Tang, Y., Jha, A.K., Shi, H., Palanivelu, R., and Allen,
1099 R.D. (2012). A novel HSI2 mutation in Arabidopsis affects the PHD-like domain and leads to
1100 derepression of seed-specific gene expression. Planta *236*, 1–17.

1101 Wang, F., and Perry, S.E. (2013). Identification of direct targets of FUSCA3, a key regulator of
1102 Arabidopsis seed development. Plant Physiology *161*, 1251–1264.

1103 Wang, L., Zhou, C.-M., Mai, Y.-X., Li, L.-Z., Gao, J., Shang, G.-D., Lian, H., Han, L., Zhang, T.-Q.,
1104 Tang, H.-B., et al. (2019). A spatiotemporally regulated transcriptional complex underlies
1105 heteroblastic development of leaf hairs in Arabidopsis thaliana. The EMBO Journal *38*, e100063.

1106 Weber, E., Engler, C., Gruetzner, R., Werner, S., and Marillonnet, S. (2011). A Modular Cloning
1107 System for Standardized Assembly of Multigene Constructs. PLOS ONE *6*, e16765.

1108 Wei, Q., Ma, C., Xu, Y., Wang, T., Chen, Y., Lü, J., Zhang, L., Jiang, C.-Z., Hong, B., and Gao, J.
1109 (2017). Control of chrysanthemum flowering through integration with an aging pathway.
1110 Nature Communications *8*, 829.

Werner, S., Engler, C., Weber, E., Gruetzner, R., and Marillonnet, S. (2012). Fast track assembly of multigene constructs using Golden Gate cloning and the MoClo system. Bioeng Bugs *3*, 38–43.

Wu, G., and Poethig, R.S. (2006). Temporal regulation of shoot development in *Arabidopsis thaliana* by miR156 and its target *SPL3*. Development *133*, 3539–3547.

Wu, G., Park, M.Y., Conway, S.R., Wang, J.W., Weigel, D., and Poethig, R.S. (2009). The sequential action of miR156 and miR172 regulates developmental timing in *Arabidopsis*. Cell *138*, 750–759.

Wu, G., Rossidivito, G., Hu, T., Berlyand, Y., and Poethig, R.S. (2015). Traffic lines: new tools for genetic analysis in *Arabidopsis thaliana*. Genetics *200*, 35–45.

Xie, Y., Zhang, Y., Han, J., Luo, J., Li, G., Huang, J., Wu, H., Tian, Q., Zhu, Q., Chen, Y., et al. (2018). The Intronic *cis* Element *SE1* Recruits *trans*-Acting Repressor Complexes to Repress the Expression of *ELONGATED UPPERMOST INTERNODE1* in Rice. Molecular Plant *11*, 720–735.

Xu, M., Hu, T., Zhao, J., Park, M.Y., Earley, K.W., Wu, G., Yang, L., and Poethig, R.S. (2016a). Developmental functions of miR156-regulated *SQUAMOSA PROMOTER BINDING PROTEIN-LIKE* (*SPL*) genes in *Arabidopsis thaliana*. PLoS Genet. *12*, e1006263.

Xu, M., Leichty, A.R., Hu, T., and Poethig, R.S. (2018). H2A.Z promotes the transcription of *MIR156A* and *MIR156C* in *Arabidopsis* by facilitating the deposition of H3K4me3. Development *145*, dev152868.

Xu, M.L., Hu, T.Q., Smith, M.R., and Poethig, R.S. (2016b). Epigenetic regulation of vegetative phase change in *Arabidopsis*. Plant Cell *28*, 28–41.

Xu, Y.M., Guo, C.K., Zhou, B.Y., Li, C.L., Wang, H.S., Zheng, B., Ding, H., Zhu, Z.J., Peragine, A., Cui, Y.H., et al. (2016c). Regulation of vegetative phase change by SWI2/SNF2 chromatin remodeling ATPase BRAHMA. Plant Physiol *172*, 2416–2428.

Yang, C., Bratzel, F., Hohmann, N., Koch, M., Turck, F., and Calonje, M. (2013a). VAL- and AtBMI1-Mediated H2Aub Initiate the Switch from Embryonic to Postgerminative Growth in Arabidopsis. Current Biology *23*, 1324–1329.

Yang, H., Howard, M., and Dean, C. (2014). Antagonistic Roles for H3K36me3 and H3K27me3 in the Cold-Induced Epigenetic Switch at Arabidopsis FLC. Current Biology *24*, 1793–1797.

Yang, L., Xu, M., Koo, Y., He, J., and Poethig, R.S. (2013b). Sugar promotes vegetative phase change in *Arabidopsis thaliana* by repressing the expression of *MIR156A* and *MIR156C*. Elife *2*, e00260.

1143 Yu, S., Cao, L., Zhou, C.M., Zhang, T.Q., Lian, H., Sun, Y., Wu, J.Q., Huang, J.R., Wang, G.D., and
1144 Wang, J.W. (2013). Sugar is an endogenous cue for juvenile-to-adult phase transition in plants.
1145 Elife *2*, e00269.

1146 Yuan, L., Song, X., Zhang, L., Yu, Y., Liang, Z., Lei, Y., Ruan, J., Tan, B., Liu, J., and Li, C. (2020). The
1147 transcriptional repressors VAL1 and VAL2 recruit PRC2 for genome-wide Polycomb silencing in
1148 Arabidopsis. Nucleic Acids Research.

1149 Yuan, W., Luo, X., Li, Z., Yang, W., Wang, Y., Liu, R., Du, J., and He, Y. (2016). A cis cold memory
1150 element and a trans epigenome reader mediate Polycomb silencing of FLC by vernalization in
1151 Arabidopsis. Nature Genetics *48*, 1527–1534.

1152 Zeng, X., Gao, Z., Jiang, C., Yang, Y., Liu, R., and He, Y. (2020). HISTONE DEACETYLASE 9
1153 Functions with Polycomb Silencing to Repress *FLOWERING LOCUS C* Expression. Plant Physiol.
1154 *182*, 555–565.

1155 Zhao, H., Lin, K., Ma, L., Chen, Q., Gan, S., and Li, G. (2020). Arabidopsis NUCLEAR FACTOR Y A8
1156 inhibits the juvenile-to-adult transition by activating transcription of MIR156s. Journal of
1157 Experimental Botany *71*, 4890–4902.

1158 Zhou, Y., Tan, B., Luo, M., Li, Y., Liu, C., Chen, C., Yu, C.-W., Yang, S., Dong, S., Ruan, J., et al.
1159 (2013). HISTONE DEACETYLASE19 interacts with HSL1 and participates in the repression of seed
1160 maturation genes in Arabidopsis seedlings. Plant Cell *25*, 134–148.

1161 Zhou, Y., Romero-Campero, F.J., Gómez-Zambrano, Á., Turck, F., and Calonje, M. (2017). H2A
1162 monoubiquitination in Arabidopsis thaliana is generally independent of LHP1 and PRC2 activity.
1163 Genome Biology *18*, 69.

1164

1165